Structural Safety 110 (2024) 102497

Contents lists available at ScienceDirect

Structural Safety

journal homepage: www.elsevier.com/locate/strusafe

Seismic fragility of unbraced industrial steel pallet racks

Marco Donà [a,*], Giacomo Piredda [a], Alberto Zonta [a], Enrico Bernardi [b], Francesca da Porto [a]

[a] Department of Geosciences, University of Padova, Via Gradenigo 6, 35131 Padova, Italy
[b] National Research Council, Construction Technologies Institute (CNR-ITC), Via Lombardia 49, 20098 San Giuliano Milanese, Milan, Italy

ARTICLE INFO

Keywords:
Industrial racking systems
Unbraced steel pallet racks
Parametric time-history analysis
3D non-linear finite-element rack modelling
Cloud analysis
Seismic fragility models

ABSTRACT

Past Italian earthquakes revealed the high seismic vulnerability of steel pallet racks designed for gravity loads only, which are still the most widespread industrial storage system. This study aims to derive the seismic fragility of these structures to enable more refined estimates of enterprise risk and the definition of effective retrofit solutions. For this purpose, 3D non-linear models of 27 unbraced pallet racks, representative of the Italian context, were analysed in Time-History under 268 bidirectional events, representative of Italian seismicity. Multiple fragility models were then derived, based on various engineering demand parameters and seismic intensity measures, through a cloud approach.

1. Introduction

Globalization and the rise of e-commerce have significantly increased the production and use of goods storage systems. Of these, standard adjustable steel pallet racks are the most common type in commercial and logistic infrastructures. These storage systems are generally made by assembling cold-formed steel profiles having thin, open cross-sections to reduce production costs and time.

In the longitudinal (down-aisle) direction, pallet racks consist of uprights, i.e., thin-walled profiles with continuous perforations, successively connected by pallet beams with a generally rectangular cross-section. These modular frames often represent the only lateral resistant system in the down-aisle direction, the stiffness and performance of which strongly depend on the beam-to-column (*btc*) connections, as well as the base connections (i.e., between uprights and industrial floor). Indeed, the insertion of longitudinal bracing systems is often avoided because of the resulting limitations in load handling. On the other hand, the lateral stability of pallet racks in the transverse (cross-aisle) direction is ensured by a series of trusses, made of horizontal and diagonal elements connecting pairs of uprights. Generally, the connections used for industrial racks are semi-rigid joints [1], whose characteristics can vary significantly from manufacturer to manufacturer, thus requiring specific experimental tests to assess their static [2] and hysteretic [3] behaviour.

The steel profiles used for these structures have cross-sections generally belonging to Classes 3 or 4 [4], and thus limited ductility. Although these profiles allow for low manufacturing and racking assembly costs, they are prone to various instability phenomena, namely to local, distortional, and global buckling (e.g., [5,6]), which must be properly verified according to standard requirements (e.g., [2]). Therefore, the use of these profiles results in a low level of displacement ductility capacity and robustness of the racking system. The poor ductility is then reflected in low values of the behaviour factor (q), which according to [3] is 1.5 for unbraced racks and can be increased to 2 when various requirements are met (especially regarding connections). The lack of robustness, on the other hand, characterises the collapse phase of these structures, which is not very predictable and can also be triggered by damage to one or a few structural elements, as often occurred following forklift collisions. The effects of the latter impacts at various upright locations and the resulting cascading effects were also investigated numerically (e.g., [7,8]).

In addition, the high slenderness of the steel profiles and the use of semi-rigid connections (conferring high deformability to the racking especially in the down-aisle direction), and the high live loads (even under service conditions) make pallet racks very vulnerable to seismic actions. Moreover, most of the racks in service today, at least in Italy, are older than the current standard for seismic design [3], and thus were designed for static loads only, resulting inadequate to withstand even limited inertial actions. Despite full awareness of this and the widespread use of racks, their seismic fragility has not yet been sufficiently investigated in the literature.

In Italy, the seismic vulnerability of pallet racks was drastically demonstrated by the 2012 Emilia-Romagna and 2016 Central Italy earthquakes [9]. The catastrophic impact of these events also highlighted the important role of racks not only in worker safety but also in

* Corresponding author.
E-mail address: marco.dona.1@unipd.it (M. Donà).

https://doi.org/10.1016/j.strusafe.2024.102497
Received 17 October 2023; Received in revised form 10 April 2024; Accepted 19 June 2024
Available online 22 June 2024

driving the economic losses of companies. Indeed, among the main mechanisms affecting businesses [10] are (*i*) physical damage to property/assets and (*ii*) business interruption (BI). Partial or total collapse of racks contributes to both of the above situations, generating direct losses due to damage to racks and stored goods, and indirect losses due to increased BI times. The latter are responsible for significant economic losses, often comparable to the reconstruction costs of warehouses [11]. Moreover, a prolonged downtime of several businesses located in the same industrial area following a seismic event could significantly impact the economy and community of that area [10,12], and this further justifies the need to evaluate the fragility of storage systems.

Recently, numerous experimental studies were conducted on rack structural elements. Some authors (e.g., [5,6]) evaluated the axial and flexural cyclic behaviour of cold-formed steel profiles with open cross-sections, investigating the respective buckling phenomena. Many other authors (e.g., [13–18]) then focused on *btc* connections, which are key elements in defining the seismic behaviour of racks. Experimental tests on these connections shown that the type of *btc* joints and the possible presence of bolted connections greatly influence the lateral behaviour of racks, making it different from that of conventional steel structures due to the pinching phenomena experienced by these joints during their cyclic response. Several numerical models were also proposed to simulate the hysteretic behaviour of *btc* connections (e.g., [16,17,19–22]). On the other hand, studies on the behaviour of base connections are less numerous. Among these, some authors [23] experimentally evaluated the seismic behaviour of these joints in the down-aisle direction; others [24] cyclically tested these joints in the cross-aisle direction, demonstrating the beneficial effect of plastic deformations occurring in the connection welds; still others [22] provided numerical models to simulate the hysteretic behaviour of these connections in the down-aisle direction and [25] proposed analytical models to determine their stiffness.

Studies in the literature also address the seismic vulnerability of the entire structural systems. For example, some authors evaluated the seismic response of storage racks with spine bracings and speed-lock connections with bolts by elastoplastic pushover analysis [21] and non-linear dynamic analysis [20]. Others [26] carried out shaking-table tests and numerical modelling of the inelastic seismic response of semi-rigid rack moment frames.

It is worth mentioning some systematic and comprehensive works aimed at providing practical recommendations and bases for standards updating. Specifically, in 2003, a panel of experts convened by the Building Seismic Safety Council, comprising practicing engineers, storage rack designers, researchers, and representatives from the Rack Manufacturers Institute, collaborated to produce FEMA 460 [27], a guidance document addressing the seismic safety of steel pallet racks in publicly accessible areas. Apart from assessing rack performance in past U.S. earthquakes and examining seismic requirements, design practices, maintenance protocols, and operational procedures, this consortium provided valuable short- and long-term recommendations to enhance existing practices and guide future standard revisions, respectively. These recommendations also stemmed from the significant, albeit limited, available experimental studies, primarily of North American origin (e.g., [28–32,13]).

Also noteworthy are the two large experimental campaigns, SEISRACKS [33] and SEISRACKS2 [34], during which several issues on the seismic behaviour of steel racks were examined through component tests, pushover tests up to collapse, and numerical simulations. SEISRACKS was based on the FEM Document 10.2.08 [35], whereas SEISRACKS2, in which more components and systems were tested, was a key contribution to the definition of EN16681 [3].

Another factor that can significantly influence the seismic vulnerability of racks by reducing their seismic stresses is the pallet sliding, as shown by some experimental campaigns [33,34,36]. Other authors [26] who investigated this effect concluded that racks with greater flexibility benefit the most, but also that this phenomenon could be detrimental, due to the potential dropping of stored goods. Furthermore, specific tests [37] indicated that the frictional coefficient at the pallet-to-rack interface varies from 0.37 to 0.45 for a wide range of pallet loads, and that the concept of inclined rack (with low inclination angle) is highly effective in reducing the risk of pallet falling.

Despite numerous studies on the seismic behaviour of racks or their components, only Gabbianelli et al. [22] and Nuñez et al. [38] evaluated their seismic fragility, using a multiple-stripe and incremental dynamic analysis approach, respectively. Gabbianelli et al. [22] derived conditional fragility on spectral acceleration (S_a) for two typical Italian rack configurations, unbraced and braced, performing non-linear dynamic analyses of 2D rack models in the down-aisle direction only. Conversely, Nuñez et al. [38] derived conditional fragility on S_a for four archetypes of Chilean pallet racks, defined by a squat-unbraced or slender-braced configuration along with a limited or large number of spans, performing non-linear dynamic analyses of 3D rack models. Recently, the incremental dynamic analysis approach was also used by Bernuzzi et al. [39] to propose a rapid seismic design method for racks, which allows both cost and key structural performance parameters to be taken into account.

Further investigation into the fragility of these structural systems is therefore needed, both for the design of effective retrofit solutions and for risk assessment of companies. Studies on the taxonomy of storage systems (e.g., [40]) are also very useful in defining homogeneous stocks of these structures, identifying common features (“attributes” or “classes”) in relation to their seismic vulnerability.

In this paper, the fragility of a stock of 27 unbraced pallet racks, characterised by various upright sections (U), load level heights (h) and total heights (H), and representative of the Italian context, was investigated. An approach based on cloud analysis and non-linear 3D rack modelling was used. In particular, the *btc* and base connections were modelled using lumped plasticity, whereas the axial and flexural behaviour of the uprights was simulated using distributed plasticity, also taking buckling into account. A friction model was also implemented under the pallet masses to simulate their possible sliding. The rack models were analysed in time-history (TH) under 268 bidirectional seismic inputs, representative of Italian seismicity on rigid soil. A specific code in the OpenSees framework was developed to handle the parametric analysis. Seismic fragility was derived both for the entire rack stock and for subsets of it, based on the main structural parameters (U, h, H). Rack fragility is provided associated with various engineering demand parameters (EDPs) and conditional on two intensity measures (IMs), i.e., S_a and PGA (peak ground acceleration), allowing for interesting comparisons. One EDP concerns the strain state of the upright sections; other EDPs describe the rack deformation in the cross-aisle direction (i.e., drift between load levels and rotations of the *btc* and base connections); lastly, triggering of pallet sliding, percentages of pallets dropped, and percentages of *btc* connections yielded were also examined as additional EDPs. Thus, the proposed approach for evaluating rack fragility is new or superior to previous studies.

2. Case study racks, structural and numerical modelling

2.1. Description of the racks and their structural model

The case studies examined in this paper are 27 unbraced steel racks designed for vertical loads only, well representative of storage systems currently used in Italian industrial buildings. These racks are double-entry, i.e., consisting of a series of double transverse frames, connected by rigid spacers in the cross-aisle direction (Y) and beams with semi-rigid connections in the down-aisle direction (X). Each transverse frame consists of two uprights and diagonal and horizontal bracing elements that connect to the uprights via bolted connections, idealized as hinges. These racks are connected to the industrial floor by connection plates anchored at the base of the uprights, which realize a bolted semi-rigid connection for rotation around the Y direction (i.e., in the

longitudinal plane) and a hinged connection for rotation around the *X* direction (i.e., in the transverse plane).

All case studies show the same plan layout, being characterized by seven spans 2700 mm long and two transverse frames 1000 mm wide, spaced 300 mm apart. In total, the racks measure 18.9 m in the *X* direction and 2.3 m in the *Y* direction, as shown in Fig. 1. The case studies differ in: (*i*) total rack height *H* (i.e., height of the top load level), equal to 6000 (H_1), 9000 (H_2) and 12,000 (H_3) mm; (*ii*) load level height *h* (or inter-story height), equal to 1000 (h_1), 1500 (h_2) and 2000 (h_3) mm; (*iii*) upright cross-sections, defined as U_1, U_2, and U_3. The latter are commonly used perforated steel profiles, the properties of which are described below. The case studies are shown in Fig. 2, along with the transverse frame bracing system. This consists of diagonal elements that reduce the effective length of the uprights to 700 mm and four horizontal elements arranged at the bottom that halve the previous spacing.

As an example, Fig. 3 shows a 3D view of the intermediate case study, i.e., the six-level rack with inter-story height of 1500 mm and total height of 9000 mm. The same figure also shows the positioning of pallet masses, which are applied on top of "dummy substructures" (according to [3]) to account for the actual height of the pallet centre of mass, which is 50 cm in this study.

The total pallet load per level and span is shown in Fig. 2 for each case study rack and was calculated based on the static bearing capacity of the transverse frame. This capacity mainly depends on the upright type, the load level height (which defines the effective length of the upright in the down-aisle direction) and the frame width (1000 mm in this study). For each type of upright, the maximum pallet load is thus a function of *h* and *H* only (or *h* and the number of levels). Therefore, all case studies are subjected to similar levels of compressive stress at the base of the uprights, and this allows to evaluate the seismic fragility of a stock of homogeneous storage systems, as well as to rationally investigate the influence of the main structural and geometric rack parameters on fragility.

Among the three load configurations indicated in EN16681 [3] for the seismic verification of racks, the fully loaded configuration was assumed in this study as the most unfavourable and representative for an overall assessment of the fragility of these structures. The other two load configurations consist of loading all levels with pallet loads 2/3 of the actual pallet loads and loading the top level only with the actual pallet loads; the latter configurations could adversely affect the rack response in the cross-aisle direction due to a significant change in the vibration modes in that direction.

The open, thin cross sections of the rack profiles generally fall into Classes 3 or 4 [4]. Whereas for a Class 3 section it is still possible to take full advantage of its strength, for a Class 4 section it is necessary to adopt its effective (or reduced) properties because of the buckling phenomena that can occur before its yielding. The cross sections of the profiles employed in this study are shown in Fig. 4, and their main inertial properties (area *A*, flexural inertia moments J_y and J_z, and torsional inertia moment J_t) are shown in Table 1, with reference to the local axes displayed in Fig. 4. Young's modulus and shear modulus of the steel are also reported in Table 1. The cross section of the beams falls into Class 3; conversely, the cross sections of the uprights and bracing elements fall into Class 4, and the related properties in Table 1 are therefore those reduced to account for local and distortional buckling [2], not explicitly modelled in this work. Instead, the global buckling of the uprights was accounted in their non-linear modelling, as described in Section 2.2.

Specifically, the beams are paired C profiles, with dimensions 150x50x9 mm and thickness 1.5 mm. The frame bracing elements (horizontal and diagonal) have a C cross section, with dimensions 35x20x9.5 mm and thickness 1.5 mm. U_1, U_2 and U_3 upright sections have similar shapes but increasing size, thickness and strength from U_1 to U_3; U_1 measures 80x100 mm and is 1.5 mm thick, whereas U_3 measures 83x130 mm and is 2.5 mm thick. Table 2 provides the effective strengths of these uprights, i.e., their axial (P_y) and flexural (M_y, M_z) capacities and the related reduction factors (χ, χ_{LT}) due to compression and flexural–torsional buckling, respectively (calculated according to [2]). For information only, the type of steel used is S275JR for pallet beams, S250GD for frame bracing elements, and S350GD for uprights.

To correctly define the structural model of the rack, however, it should be considered that the actual stiffness of the frames is considerably lower than that obtainable from a truss model composed of the actual bracing profiles. This is due to the clearances that characterize the *btc* connections. To overcome this issue, a reduced cross-sectional area of the diagonals ($A_{d,red}$) can be adopted, as suggested by EN15512 [2]. For the racks investigated here, $A_{d,red}$ was estimated based on previous experimental results [41], and its value is also shown in Table 1.

In order to account for the combined effect of axial and bending stresses on the upright in a modelling approach that simulates the various non-linear section behaviours separately (as will be shown in Section 2.2), a reduction in the flexural capacity of the upright equal to its axial compression ratio (i.e., ratio of vertical load to axial capacity) was assumed, which depends substantially on the spacing between the load levels (*h*). This reduction was approximately 40 %, 35 % and 30 % for cases with *h* equal to 1.0, 1.5 and 2.0 m, respectively. For convenience, the values of the reduced flexural capacities ($M_{y,red}$, $M_{z,red}$) of the various uprights are also shown in Table 2.

Regarding the beam-to-column (*btc*) connections, two types of joints were employed: *btc1* for the U_1 and U_2 uprights (which have similar section height, i.e., 100 mm), and *btc2* for the U_3 upright (which has greater height, i.e., 130 mm). The main performances of these joints, in terms of rotational stiffness (k_φ) and strength (M_φ), are shown in Table 3

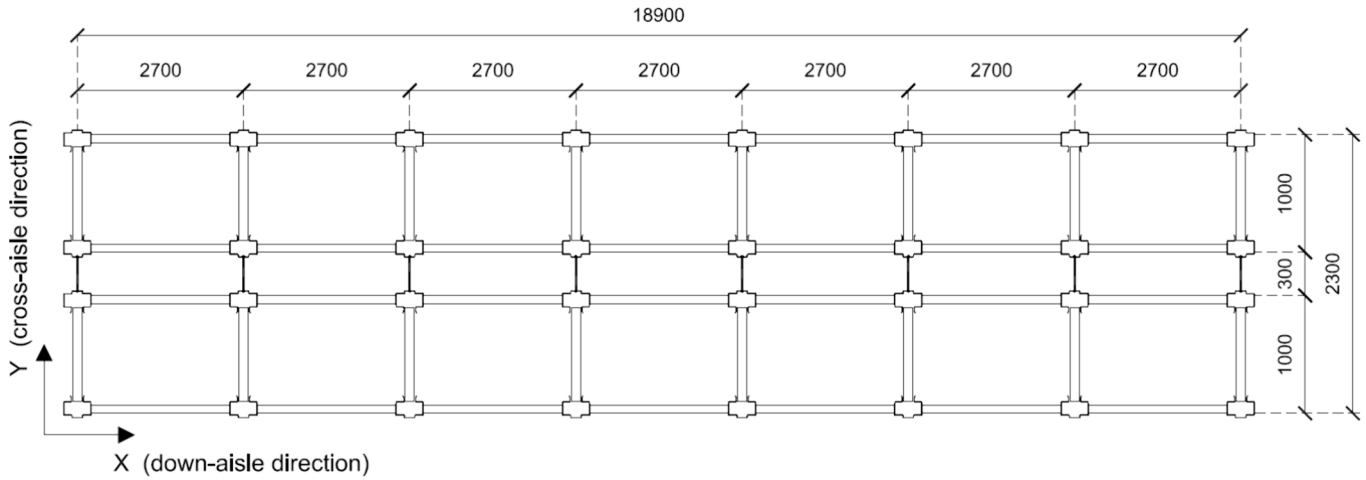

Fig. 1. Plan layout of all case study racks.

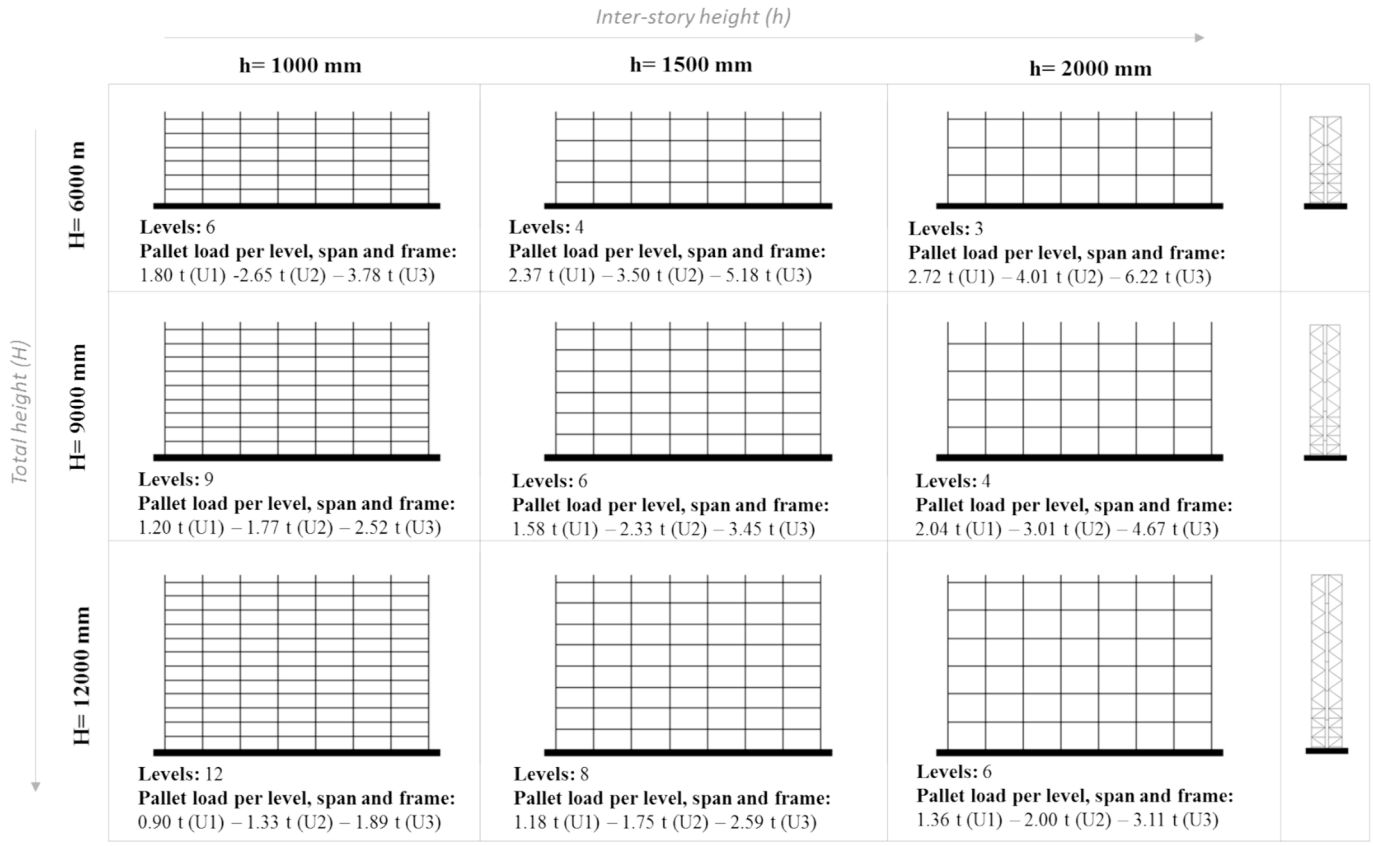

Fig. 2. Case study racks: geometric configurations for each type of upright (U_1, U_2, and U_3).

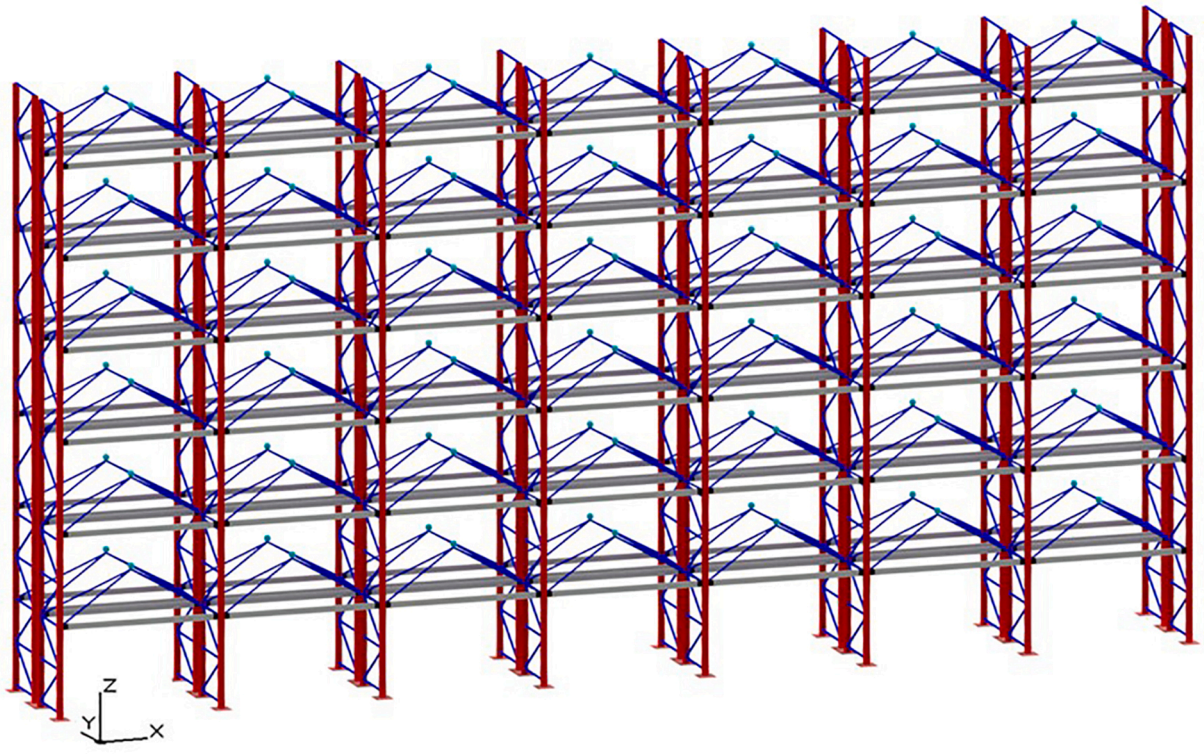

Fig. 3. Global view of the intermediate case study rack: 7 spans, 6 load levels, $h = 1.5$ m and $H = 9$ m.

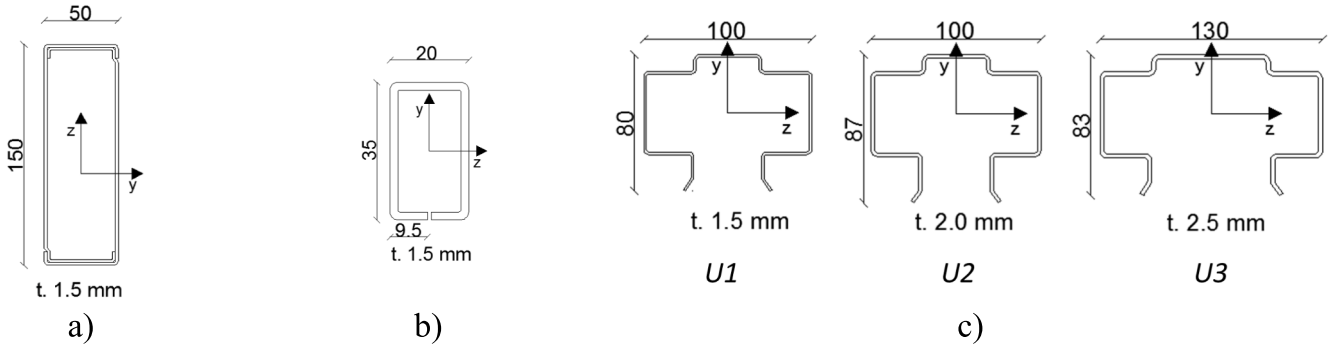

Fig. 4. Cross sections of: (a) pallet beams; (b) diagonals/horizontal frame elements; (c) uprights.

Table 1
Inertial properties of the rack profiles.

		A [cm^2]	$A_{d,red}$ [cm^2]	J_t [cm^4]	J_y [cm^4]	J_z [cm^4]	E [MPa]	G [MPa]
Pallet beams		8.12	–	131.23	273.90	35.80	210,000	80,769
Frame bracing elements		1.53	0.38	0.01	0.80	1.86	210,000	80,769
Uprights	U_1	3.62	–	0.03	47.14	26.10	210,000	80,769
	U_2	5.44	–	0.08	62.00	37.00	210,000	80,769
	U_3	7.57	–	0.18	149.50	64.20	210,000	80,769

and derive from experimental tests. Table 3 also shows the same information for the base joints, which derive from Gabbianelli et al. [22]. In particular, the yield ($M_{\varphi y,Y}$) and peak ($M_{\varphi p,Y}$) strengths reported in Table 3 refer to the rotation around the Y axis (i.e., in the longitudinal plane) and were used to calibrate the non-linear hysteretic models of the connections (see Section 2.2).

2.2. Presentation of the 3D finite-element models

A MATLAB code was compiled to automatically generate the geometries of the selected racks and a Tcl code was developed to transform these geometries into Finite-Element (FE) models and perform Time-Histories (TH) analyses in the OpenSees software framework [42]. This parametric modelling approach made it possible to appropriately handle many structural analyses on various pallet racks, necessary to assess their seismic fragility.

A peculiarity of racks, at least of those unbraced, is their high flexibility, which results in large displacements under seismic action; these, together with the high service loads, produce significant second-order effects. EN16681 [3] requires such effects to be considered when the critical load multiplier α_{cr} is less than 10, as in all case studies. To this end, the *P-Delta* formulation implemented in OpenSees was adopted, which allows for geometric non-linearities to be taken into account.

The non-linear 3D FE models of the racks were implemented using the OpenSees element objects described in Table 4. In general, material non-linearities were considered for the uprights, by means of distributed

Table 2
Axial (P_y), flexural (M_y, M_z) and reduced flexural ($M_{y,red}$, $M_{z,red}$) capacities of the uprights, and associated buckling (χ) and flexural–torsional buckling (χ_{LTy}, χ_{LTz}) factors.

Upright	h [m]	P_y [kN]	χ [–]	M_y [kN•cm]	$M_{y,red}$ [kN•cm]	M_z [kN•cm]	$M_{z,red}$ [kN•cm]	$\chi_{LTy} = \chi_{LTz}$ [–]
U_1	1.0	126.7	0.911	347.0	208.2	202.0	121.2	0.996
	1.5		0.841		225.6		131.3	0.998
	2.0		0.749		242.9		141.4	0.996
U_2	1.0	190.4	0.900	462.0	277.2	279.0	167.4	0.996
	1.5		0.821		300.3		181.4	0.998
	2.0		0.718		323.4		195.3	0.996
U_3	1.0	265.0	0.936	879.0	527.4	427.0	256.2	0.996
	1.5		0.888		571.4		277.6	0.998
	2.0		0.825		615.3		298.9	0.996

Table 3
Rotational stiffnesses and strengths of the beam-to-column (*btc*) and base joints.

	$k_{\varphi,X}$ [N•mm/rad]	$k_{\varphi,Y}$ [N•mm/rad]	$k_{\varphi,Z}$ [N•mm/rad]	$M_{\varphi y,Y}$* [N•mm]	$M_{\varphi p,Y}$* [N•mm]
btc1 joint (U_1, U_2)	fixed	$1.17{\cdot}10^8$	$1.17{\cdot}10^8$	$1.13{\cdot}10^6$	$1.69{\cdot}10^6$
btc2 joint (U_3)	fixed	$1.80{\cdot}10^8$	$1.80{\cdot}10^8$	$1.34{\cdot}10^6$	$2.01{\cdot}10^6$
base joint	hinged	$4.35{\cdot}10^8$	fixed	$2.61{\cdot}10^6$	$5.22{\cdot}10^6$

* In the case of *btc* connections, these values refer to hogging; the respective values in sagging are reduced to 90%.

Table 4
OpenSees objects implemented for the various rack elements.

Rack elements	OpenSees objects	Description
Uprights	Force-Based Beam-Column Elements	Hysteretic asymmetrical axial behaviour via *uniaxialMaterial Pinching4* object (Fig. 5a), accounting for buckling. Elasto-plastic flexural behaviour. Five integration points along each element.
Frame bracing elements	Beam With Hinges Elements	Linear elastic beams with stiffnesses from Table 1 and end hinges to simulate truss-like behaviour.
Spacers	Elastic Beam Column Elements	Linear elastic beams with equivalent stiffnesses.
Pallet beams	Elastic Beam Column Elements	Linear elastic beams with stiffnesses from Table 1.
Btc connections	Zero-Length Elements	Hysteretic rotational behaviour around *Y* axis via *uniaxialMaterial Hysteretic* object (Fig. 5b). Linear elastic rotational behaviour around *Z* axis with stiffnesses from Table 3. Rotation around *X* axis equal to that of the beam.
Base connections	Zero-Length Elements	Hysteretic rotational behaviour around *Y* axis via *uniaxialMaterial Hysteretic* object (Fig. 5c). Rotational stiffness around *X* axis released. Rotation around *Z* axis equal to that of the upright.
Mass substructures	Elastic Beam Column Elements	Linear elastic beams with stiffnesses that simulate truss behaviour and do not affect modal results.
Pallet-support contact	Zero-Length Element	Equivalent friction model (Fig. 5d) with penalty stiffness before sliding and perfectly plastic behaviour for the sliding phase.

plasticity, and for the beam-to-columns and base connections, by means of concentrated plasticity. The other elements, i.e., the horizontal/diagonal bracing profiles, the spacers, and the pallet beams, were modelled as linear elastic elements. As mentioned above, the pallet mass is modelled by means of a lumped mass at the pallet's centre of gravity, supported by a dummy elastic substructure. In addition, a friction model between pallet mass and substructure was implemented to simulate the possible sliding of the pallet on the support beams. A more detailed discussion of the various components of the rack model follows.

The *Force-Based Beam-Column Element* was implemented for the uprights. Four to six integration points are required to achieve sufficient accuracy in computing the curvature distribution along the element [43,44]. Thus, five integration points and the Gauss-Lobatto integration scheme were assumed, assigning the same force–deformation model to all integration sections. In particular, a specific behaviour was defined for each degree of freedom (DOF) of the section through the *uniaxialMaterial* object, which allows various uniaxial stress–strain relationships to be defined. Therefore, six stress–strain laws were defined to represent the global behaviour of the upright section.

Regarding the axial behaviour of the upright section, reference was made to the results of Padilla-Llano et al. [5], who experimentally evaluated the axial behaviour of structural framing members, consisting of cold-formed steel profiles with open (C-shaped) cross-sections, by applying a cyclic axial loading protocol adapted from FEMA 461 [45]. These results showed an asymmetrical axial behaviour of these elements. In tension (positive range of axial load P in Fig. 5a), these elements reach their yield strength (P_y), after which they exhibit a very short hardening branch and a subsequent degrading behaviour. In compression (negative P values), these elements do not reach their yield strength due to buckling effects, and their strength degradation after the peak value ($\chi \cdot P_y$) is much more abrupt than that in tension. Furthermore, the axial load-deformation (P-ε) response of these elements is characterised by evidently pinched hysteretic cycles. This behaviour was modelled in OpenSees by means of the *uniaxialMaterial Pinching4* object, whose non-linear hysteretic law is shown in Fig. 5a, normalised to the values of load and strain at yield (P_y and ε_y). Pinching parameters were assumed consistent with [5], while P_y, χ and ε_y derive from Tables 1 and 2.

As for the flexural behaviour around both in-plane axes of the upright section, an elastoplastic model was assumed, calibrated to the reduced flexural capacities ($M_{y,red} \cdot \chi_{LT}$ and $M_{z,red} \cdot \chi_{LT}$) given in Table 2 and the inertial properties given in Table 1. In OpenSees, this behaviour was simulated through the *uniaxialMaterial Steel02* object, which implements the Giuffrè-Menegotto-Pinto stress–strain model [46]. Although the actual flexural behaviour of these steel profiles exhibits strength degradation beyond yielding, as shown by some experimental evidence (e.g., [6]), the elastoplastic model is an acceptable approximation in favour of greater numerical stability and was also assumed by other authors (e.g., [22]). In fact, once the flexural capacity of the uprights is exceeded, inter-story drifts increase rapidly, resulting in plasticization of the *btc* connections (if not already occurred) and axial instability of the upright. Furthermore, pushover tests on real racks [34] showed the existence of some rotational ductility for this type of structures, albeit limited compared to conventional steel structures. Lastly, for the torsional and shear behaviours of the upright section, linear elastic models were implemented using the *uniaxialMaterial Elastic* object, calibrated to the stiffnesses defined in Table 1.

The horizontal/diagonal bracing elements, spacers, and pallet beams were modelled as linear elastic beams, albeit with different approaches. The bracing elements were implemented through the *Beam With Hinges Element* object, which allows different sections to be defined between the inner part of the element and its ends. In particular, the end sections were concentrated and without flexural stiffness to simulate a truss-like behaviour; the other stiffnesses of the end sections, as well as the stiffnesses of the inner part of these elements, derive from Table 1. On the other hand, spacers and pallet beams were implemented via the *Elastic Beam Column Element* object, which simulates conventional elastic beam behaviour, calibrated to the inertial properties in Table 1.

The *btc* connections were modelled by rotational plastic hinges in the upright-beam joints, using the *Zero-Length Element* object. The behaviour of these connections depends on the axis of rotation, and the main one is rotation around the Y axis, i.e., in the longitudinal plane of the rack. Experimental studies (e.g., [14,16,17]) showed that this behaviour can be modelled by an elastoplastic backbone curve with hardening after yielding and strong strength degradation upon exceeding the peak moment, which is significantly greater than the yield moment; in addition, the cyclic moment-rotation (M_φ-φ) response of these connections is characterised by some pinching.

This non-linear behaviour, implemented in OpenSees through the *uniaxialMaterial Hysteretic* object, is shown in Fig. 5b. Specifically, the hysteretic law and pinching parameters were taken from Gabbianelli et al. [22], whereas the yield ($M_{\varphi y,Y}$) and peak ($M_{\varphi p,Y}$) strengths of the *btc1* and *btc2* connections are defined in Table 3. Conversely, the rotational behaviour of these connections around the Z axis was assumed linear in the absence of specific tests, with rotational elastic stiffness $k_{\varphi,Z}$ given in Table 3. Lastly, the rotation around the X axis was set equal to the torsional rotation of the beams, via the *EqualDOF command* of OpenSees.

The base connections were modelled similarly, i.e., through the *Zero-Length Element* object and the *Hysteretic* material for rotation about the Y axis, which is the main behaviour for these connections as well. The specific non-linear hysteretic response is shown in Fig. 5c. The skeleton curve and pinching parameters were also taken from Gabbianelli et al. [22], whereas the yield ($M_{\varphi y,Y}$) and peak ($M_{\varphi p,Y}$) strengths are specified in Table 3. Then, for these connections, the rotation around the X axis was released, while the rotation around the Z axis was set equal to the torsional rotation of the uprights, using the *EqualDOF command*.

To properly simulate the inertial actions due to pallet loads, a pair of

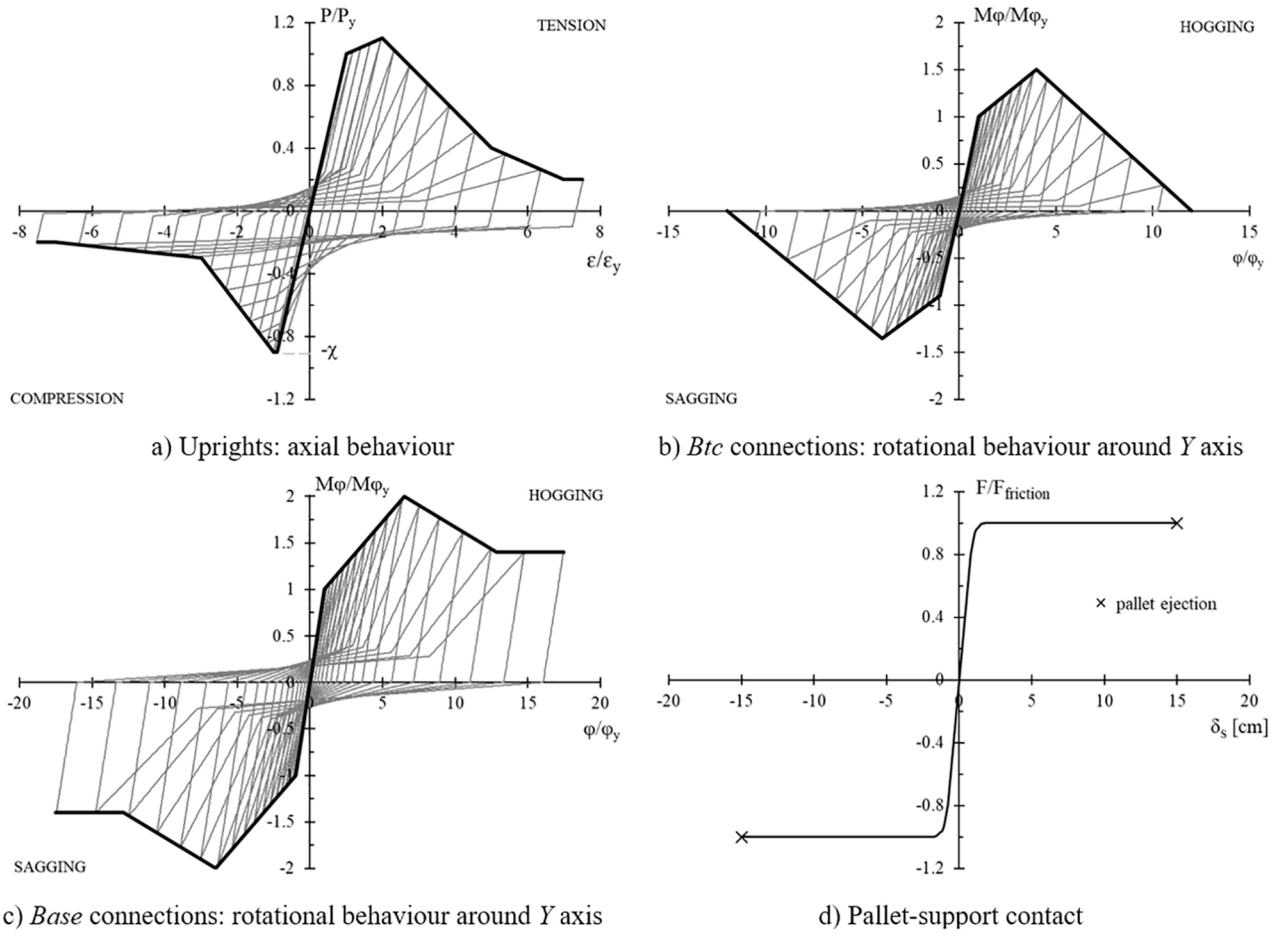

Fig. 5. Non-linear hysteretic laws used in the FE modelling of racks.

nodes was introduced at the centre of gravity of each pallet. The lumped mass of the pallet (whose values are provided in Fig. 2 for the various case studies) was applied to the upper node, while the lower node was used to create the dummy substructure, as shown in Fig. 6. Then, through the *Zero-Length Element* object, a friction model was implemented between the two nodes to simulate the possible sliding of pallets in the cross-aisle direction. Specifically, the *uniaxialMaterial Steel01* was used as the friction model, and its non-linear law is shown in Fig. 5d. The friction force $F_{friction}$ was calculated according to the Coulomb model, being proportional to the pallet weight and the friction coefficient μ_s; the latter was set equal to 0.37, which is a representative value of wood-steel friction [3]. The penalty stiffness was calibrated as 10^5N/mm through a preliminary parametric analysis; significantly lower stiffnesses would interact with the dynamics of the rack (changing the modal results), whereas higher stiffnesses could result in numerical instabilities during the analysis. The inertial forces are transmitted to the rack through the dummy substructure, which consists of four *Elastic Beam Column Elements* arranged in a pyramid pattern (see Fig. 6). To avoid the rigid plane effects that might result from these substructures, very low shear, flexural, and torsional stiffnesses were assigned to the cross section of these elastic beams. Lastly, an algorithm was also implemented in OpenSees to record the displacement of pallets and to remove them when the limit displacement of 150 mm was exceeded. This limit was set on the basis of the frame (1000 mm) and pallet (1200 mm) width; indeed, before losing either support, the pallet can slide on each side for 100 mm plus the beam width, which is 50 mm.

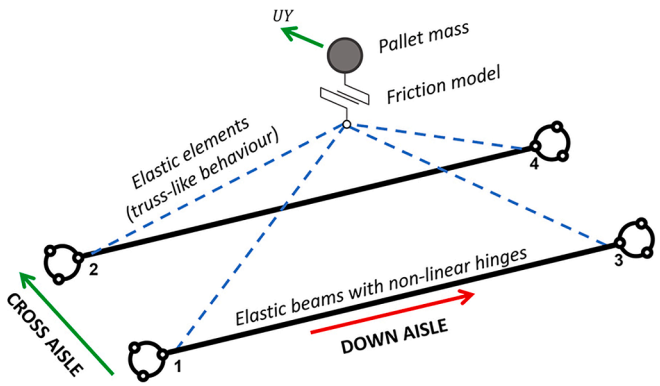

Fig. 6. Representation of the dummy substructure and pallet sliding model.

It is worth considering that OpenSees (as well as many other FE software) does not allow the implementation of the seventh degree of freedom [47] to account for the effects of warping or Bi-moment, i.e., the coupling of flexural and flexural–torsional behaviour. As studied by Bernuzzi et al. [48], this phenomenon could significantly increase the stresses in typical racking profiles, and this increase depends mainly on the geometric configuration of the frame, the degree of flexural stiffness associated with beam-to-column joints (ρ), the distance between load levels, and the class of steel. Specifically, ρ is the ratio between the actual rotational stiffness of *btc* joints and the transition stiffness between flexible and semi-rigid joints, calculated according to EN1993-1-8 [1].

For the case study racks, ρ ranges from 1.1 to 1.7. Considering these values of ρ and a steel type S350, the stress increment in the uprights is always less than 5 % according to the findings in [48] (for steel profiles

Table 5
Inertial properties of the net sections of the rack profiles used in the benchmark test [33].

	A [cm^2]	t [mm]	J_y [cm^4]	J_z [cm^4]	W_y [cm^3]	W_z [cm^3]
Pallet beams (*TG 130×45×1.5 mm*)	6.98	1.5	174.22	16.87	26.79	5.17
Uprights (*100/20b*)	5.26	2.00	69.47	40.61	14.32	8.33

similar to those in this study), with the greatest increment in the case of maximum inter-storey height (i.e., 2.0 m). Furthermore, the racks analysed here are double-entry, thus less prone to torsional effects than the single-entry racks analysed in [48]. Therefore, although the warping effects should generally be taken into account for the verification of racks, in this study these effects can be reasonably neglected in favour of greater calculation simplicity.

This simplification is also in line with the purpose of the study, which is to assess the seismic fragility of a consistent set of pallet racks rather than to verify a specific rack structure. In this sense, this approximation could be encompassed within the epistemic uncertainties. For more information on the warping influence, please refer to Bernuzzi et al. [47,48].

2.3. Validation of the rack modelling approach

In order to assess the effectiveness of the overall rack modelling approach, a comparison was made between the experimental response of a full-scale rack specimen, subjected to incremental cyclic displacements in the down-aisle direction during the SEISRACKS experimental campaign [33], and its numerical prediction using the modelling strategies discussed in Section 2.2.

The test specimen is a single-entry steel pallet rack consisting of two spans 1800 mm long and three load levels 2000 mm apart. The load applied on the beams to simulate the pallet weight is 17 KN per span and level. The steel profiles of beams and uprights employed in the benchmark test are similar to those used in this study, albeit with different dimensions. The main inertial characteristics of the net sections of these profiles are shown in Table 5 and refer to the Cartesian axes shown in Fig. 4. The axial and bending capacities of beams and uprights were derived from their inertial characteristics, considering the use of a S275 type steel.

As regards the *btc* connection, it was previously tested by means of a monotonic test [33]; the experimental values of its initial stiffness ($k_{\varphi,Y}$), yield and peak strengths ($M_{\varphi y,Y}$, $M_{\varphi p,Y}$), and yield and peak rotations ($\varphi_{y,Y}$, $\varphi_{p,Y}$) are given in Table 6. In line with the assumptions in this study, the experimental response of this joint is different between hogging (*130 MB-3*) and sagging (*130MT-3*). Fig. 7a shows the comparison between this experimental response and that of the corresponding numerical model (see Fig. 5b), appropriately recalibrated.

Regarding the base connection, various specimens and load conditions were tested in SEISRACKS [33]. For the purposes of this validation, the test conducted on the specimen simply bolted to a steel deck (*SBDCF25-1*) and subjected to an axial load of 25kN and incremental bending cycles in the down-aisle direction was assumed, as this is the joint used in the rack test. A similar bending test was also conducted on a connection bolted to a concrete deck (*CBDCF25-1*), which would be more similar to the base joint analysed in this parametric study. The cyclic response of both connections is shown in Fig. 7b, along with the response of the corresponding numerical model (see Fig. 5c), appropriately recalibrated. Consistently with the assumptions in this study, the behaviour of the base joint was modelled as symmetric, and therefore the calibration was based on the average behaviour between those in hogging and sagging. Although the hysteric shape of the adopted model ("*uniaxialMaterial Hysteretic*", see Section 2.2) better represents bolted connections to concrete decks, through appropriate calibration, it also allowed a sufficiently faithful prediction of the behaviour of connection SBDCF25-1.

The data provided in SEISRACKS [33] concerning the benchmark test were adequate to thoroughly characterise the numerical rack model in OpenSees and, when specific details were lacking, reliance was placed on the assumptions outlined in the previous subsections. Lastly, Fig. 7c illustrates the comparison between the experimental cyclic response of the rack specimen and its numerical simulation using the adopted modelling approach. Overall, the comparison is very good, even considering the uncertainties related to the non-linear behaviour of the connections, which significantly influence the lateral response of the rack.

3. Method of seismic fragility assessment

3.1. Engineering demand parameters and damage states

To describe the damage of a structural system, it is necessary to refer to specific performance parameters or engineering demand parameters (EDPs), selecting threshold values for these that represent damage states (DSs) of increasing intensity. Four main EDPs were evaluated in this study, i.e., an overall strain parameter (axial and flexural) of the uprights (ε^*), the maximum drift between load levels in the down-aisle direction (θ_X), and the maximum rotations of the *btc* (φ_{btc}) and base (φ_{base}) connections around the Y axis.

Three increasing levels of damage were defined for each EDP, i.e., DS1, DS2 and DS3. DS1 represents an incipient damage condition, with structural behaviour still in the elastic range. DS2 indicates a yielding condition, where the safety of the rack users is still ensured; therefore, DS2 is like a Life Safety limit state. Lastly, DS3 corresponds to a condition where the safety of the operators is no longer guaranteed, which can rapidly degenerate into partial or total collapse of the rack.

The EDP ε^* is defined in Eq. (1) and is the sum of the following addends: ratio of actual axial strain (ε_p) to reduced yield axial strain (i.e., $\varepsilon_{p,y}\cdot\chi_P$); ratio of actual curvature about the local Y-axis (χ_Y) to related yield curvature ($\chi_{Y,y}$); ratio of actual curvature about the local Z-axis (χ_Z) to related yield curvature ($\chi_{Z,y}$). Eq. (1) is similar to the conventional and code-compliant formula for safety checks of steel profiles subjected to compression and biaxial bending, except that it is expressed in strain instead of force, allowing for increasing values even after section

Table 6
Initial stiffness, strengths and rotations of the *btc* joints used in the benchmark test [33].

	$k_{\varphi,Y}$ [N•mm/rad]	$M_{\varphi y,Y}$ [N•mm]	$\varphi_{y,Y}$ [mrad]	$M_{\varphi p,Y}$ [N•mm]	$\varphi_{p,Y}$ [mrad]
btc joint (*130MB-3*, hogging)	$0.96\cdot10^8$	$2.53\cdot10^6$	26.0	$3.14\cdot10^6$	129.7
btc joint (*130MT-3*, sagging)	$1.19\cdot10^8$	$2.11\cdot10^6$	18.8	$2.44\cdot10^6$	107.3

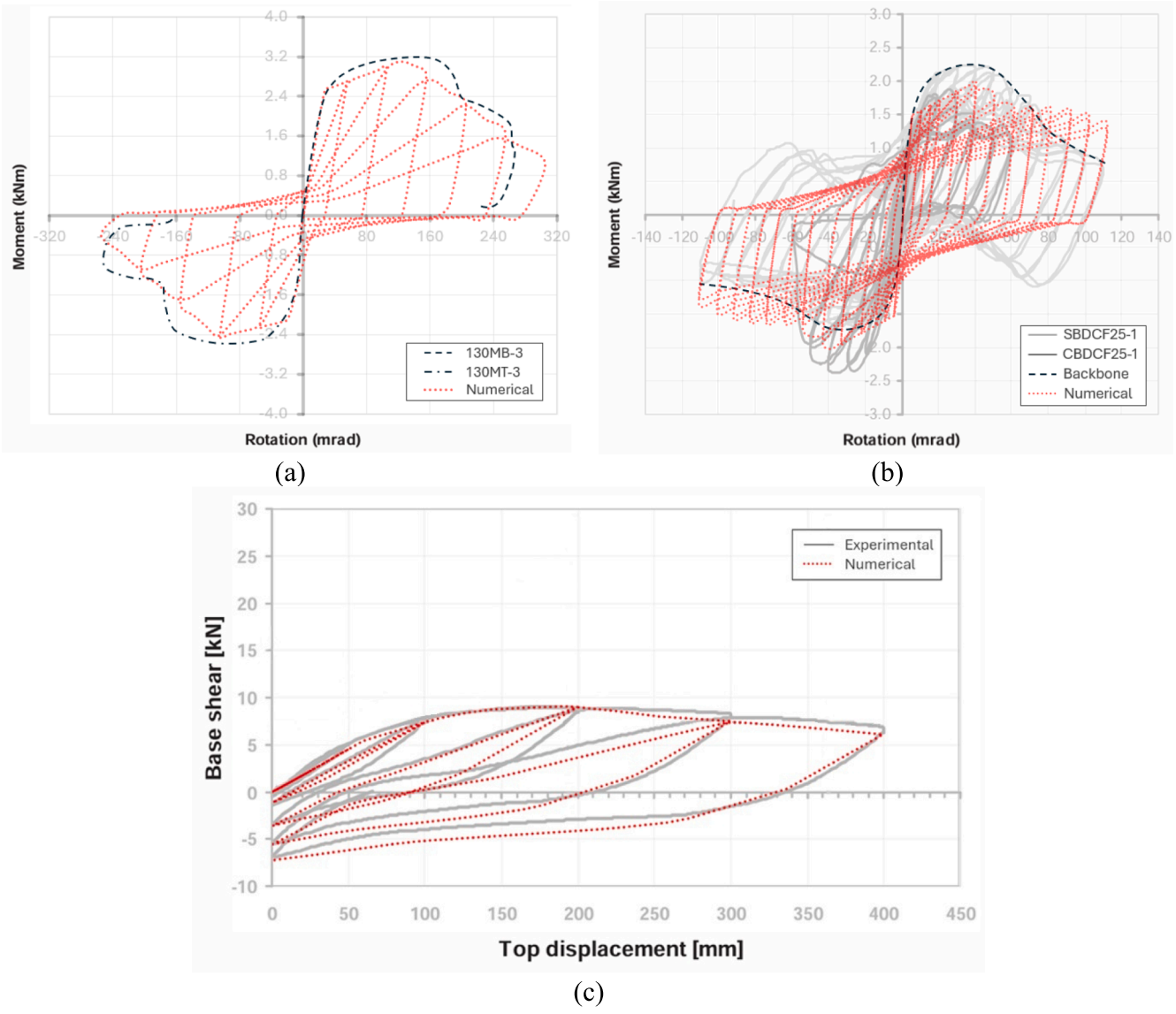

Fig. 7. Comparison of the experimental and numerical responses of: (a) *btc* joint; (b) base joint; (c) benchmark rack specimen (experimental data from [33]).

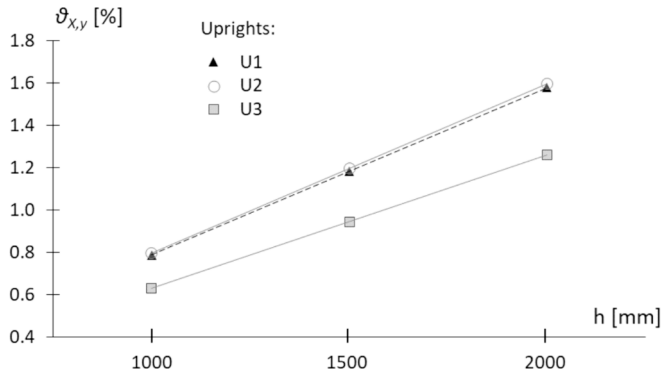

Fig. 8. Yield drift of the uprights in the X direction ($\theta_{X,y}$), depending on the type of section (U_1, U_2, U_3) and the height between load levels (h).

yielding. ε^* was recorded on all significant cross sections of the uprights and in all analysis steps, and its maximum value was then assumed for each analysis.

Table 7
Thresholds for defining DSs of selected EDPs.

EDP	DS1	DS2	DS3
ε^*	$\geq$0.8<	$\geq$1.0<	$\geq$1.5
θ_X	$\geq$0.8 $\theta_{X,y}$<	$\geq$1.0 $\theta_{X,y}$<	$\geq$1.5 $\theta_{X,y}$
φ_{btc}	$\geq$ 0.8 $\varphi_{btc,y}$<	$\geq$1.0 $\varphi_{btc,y}$<	$\geq\varphi_{btc,p}$ = 4.0 $\varphi_{btc,y}$
φ_{base}	$\geq$0.8 $\varphi_{base,y}$ <	$\geq$1.0 $\varphi_{base,y}$<	$\geq\varphi_{base,p}$ = 6.5 $\varphi_{base,y}$

$$\varepsilon^* = \frac{\varepsilon_P}{(\varepsilon_{P,y} \cdot \chi_P)} + \frac{\chi_Y}{\chi_{Y,y}} + \frac{\chi_Z}{\chi_{Z,y}} \quad (1)$$

Regarding θ_X, its values are significant when related to the yield drift ($\theta_{X,y}$) of the uprights in the specific case of analysis. Therefore, the values of $\theta_{X,y}$ were estimated using the classical elastic beam theory, based on the yield curvature ($\chi_y = M_y/EJ_y$) of the uprights and their static scheme in the X-direction, assuming a degree of connection (encastre) for the *btc* joints of 35 % (a representative value for the case study racks). The estimated values of $\theta_{X,y}$ are shown in Fig. 8 for various uprights and heights between load levels.

The lateral force–displacement response of racks is generally

characterised by a relatively short and unstable plastic branch, and EN16681 [3] allows the use of behaviour factor (q) values up to 1.5 for unbraced racks. Slightly higher values, up to 2, can be used when several requirements are met, including the type of connection hooking (which greatly influences the limited displacement ductility of the racks). Higher values of q can be taken only if demonstrated by specific experimental tests (as in SEISRACK2 [34]). Therefore, based on these considerations, the threshold for defining DS3 was conservatively set as 1.5 for ε^* and $1.5{\cdot}\theta_{X,y}$ for θ_X, as shown in Table 7. Reasonable variations in these thresholds, however, do not result in significant changes in fragility, because ε^* and θ_X values increase very quickly after the yield condition is reached. Then, DS1 is attained when $\varepsilon^* \geq 0.8$ and $\theta_X \geq 0.8{\cdot}\theta_{X,y}$, and DS2 when $\varepsilon^* \geq 1.0$ and $\theta_X \geq \theta_{X,y}$.

Lastly, as shown in Table 7, the DSs associated with the *btc* and base connections were defined based on their rotations at yield ($\varphi_{btc,y}$ and $\varphi_{base,y}$) and peak strength ($\varphi_{btc,p}$ and $\varphi_{base,p}$). The yield rotations were calculated from the yield strength and rotational stiffness values given in Table 3, whereas the rotations at peak strength are shown in Fig. 5 ($\varphi_{btc,p} = 4.0{\cdot}\varphi_{btc,y}$, $\varphi_{base,p} = 6.5{\cdot}\varphi_{base,y}$).

While ε^* is the EDP that best represents or drives structural collapse (as will be demonstrated in the next section), the other EDPs allow for a detailed assessment of the damage mode of the racking system. It is then worth noting that reaching DS3 for any of the EDPs analysed is generally associated with partial collapse (i.e., failure of a single structural element). However, for these structures, a partial collapse can often represent a condition of incipient global collapse, given their low level of structural redundancy and robustness, and the important cascading effects that can be triggered from local failures.

Since bidirectional analyses were conducted, attention should be paid to the correlation between EDP and IM values. In particular, θ_X, φ_{btc}, and φ_{base} are global deformation parameters in the down-aisle direction and therefore must be associated with IM values in the same direction (X). On the other hand, ε^* is a strain parameter of uprights dependent on axial compression and biaxial bending, so its association with a certain IM direction is not straightforward. However, the racks considered here are characterized by much stiffer behaviour in the cross-aisle direction than in the down-aisle direction, which implies, for the same event in the two directions, higher seismic accelerations and thus higher inertial forces in the Y direction. Therefore, ε^* values were correlated with IM values in the cross-aisle direction, and the adequacy of this assumption will be proven by the fragility results.

In addition to the main EDPs, other parameters were evaluated to provide insights into the possible loss of stored pallets and the damage propagation to *btc* connections. Specifically, fragility curves were derived to estimate the probability of triggering pallet sliding, dropping certain pallet volumes (as % of total stored pallets), and yielding certain amounts of *btc* connections (as % of total *btc* connections). This was made possible by parametric coding in OpenSees, which allowed automatic controls on pallet mass displacement to be implemented for each analysis step. More information will be provided directly in subsection 4.3, presenting these fragility results.

3.2. Cloud analysis

Various approaches exist to estimate fragility functions from TH results [49], including incremental dynamic analysis (IDA), multiple strip analysis (MSA), and cloud analysis. In this study, cloud analysis was selected for the following advantages. Firstly, it employs unscaled ground motion records of various intensities, unlike IDA and MSA, which rely on records scaled to predefined intensity measure (IM) values, and thus require more TH analyses to achieve statistically significant data for each IM level. Secondly, cloud analysis offers simpler procedures for deriving fragility parameters and enables estimation of conditional fragility on various IMs without extensive reprocessing. In addition, the availability of a reliable seismic database, representative of Italian seismicity (see subsection 3.3), was another key factor in choosing the approach.

The method of moments [50] was used as statistical inference method to derive the parameters of the fragility curve associated with each damage state (DS_i), i.e., the mean ($\mu_{DS,i}$) and logarithmic standard deviation ($\beta_{DS,i}$) of the lognormal cumulative density function (CDF).

The fragility curves associated with the various EDPs and DSs were obtained by processing the TH results of the analyses with numerical convergence. Indeed, in the case of non-convergence, the EDPs may not have reached the DSs only because of the early termination of the analysis, which therefore provides partial information only. However, to correctly estimate the probability of rack failure, information from non-convergent analyses was also used according to [50,51,52]. Specifically, it was assumed that structural collapse is realised through two independent conditions: (*i*) attainment of DS3 for EDP ε^* in the case of numerical convergence (Conv); (*ii*) termination of the TH analysis due to numerical non-convergence (NonC). The latter hypothesis is well justified by the fact that non-convergence always occurred in the presence of excessive strains of the upright sections, thus resulting in a condition of global dynamic instability. Therefore, the actual probability of rack collapse can be estimated by the total probability theorem as shown in Equation (2), where the probability of reaching DS3 in the case of non-convergence ($P\,(D \geq DS_3|IM,\, NonC)$) is taken as 1 and the probability of non-convergence ($P\,(NonC|IM)$) is estimated by the logistic regression model in Equation (3), where α_0 and α_1 are the calibration parameters.

$$P(D{\geqslant}DS_3|IM) = P(D{\geqslant}DS_3|IM, Conv){\cdot}(1 - P(NonC|IM)\,) + \\ +P(D{\geqslant}DS_3|IM, NonC){\cdot}P(NonC|IM) \tag{2}$$

$$P(NonC|IM) = \frac{1}{1 + e^{-(\alpha_0+\alpha_1{\cdot}\ln(IM))}} \tag{3}$$

3.3. Database of selected ground motions

A set of natural records was selected from the database provided by Paolucci et al. [53] as part of the national cooperative project ReLUIS-DPC 2019–2021 (WP4–MARS: Seismic Risk Maps). This database was derived from the SIMBAD dataset [54] through a selection and spectral matching procedure, specifically developed in the previous project to collect seismic signals suitable for deriving fragility curves via cloud approach [52]. This selection is based on similarity criteria with Italian code-compliant spectra [55], defined for rigid (type A-B) and soft (type C-D) soils and for various return periods (T_R, from 50 to 10,000 years). The similarity criteria were assumed to be less stringent than strict spectral compatibility [55], with the goal of obtaining a set of site-independent earthquakes.

Specifically, the set of records selected for this study includes 134 unscaled bidirectional events, which are representative for rigid soils and cover a range of T_R from 50 to 5,000 years. The PGA values of the two horizontal components (Hc_1 and Hc_2) of each event are shown in Fig. 9a. These events were applied considering the Hc_1 component acting first along the X direction and then along the Y direction, thus performing 268 TH analyses for each case study rack (7236 in total).

Two IMs were used in this study, S_a and PGA. S_a depends on the dynamic characteristics of the structure and better represents the actual seismic acceleration experienced by the racks than PGA; hence, it is more rational than PGA to represent the seismic fragility of these flexible structures. In contrast, PGA is structure-independent and thus allows fragility to be expressed in a more general way (since knowledge of the main vibration period of racks is not required); furthermore, PGA is commonly employed to define seismic hazard maps and conduct large-scale risk analyses, making it potentially more practical for rapid risk assessments of industrial sites (including rack stocks).

Fig. 9b shows the S_a values associated with the main vibration period of the racks in the down-aisle direction ($T_{1,X}$) and in the cross-aisle direction ($T_{2,Y}$). This figure is much more populated than Fig. 9a, since a single component (Hc_1 or Hc_2) of a seismic event returns 2xN values of

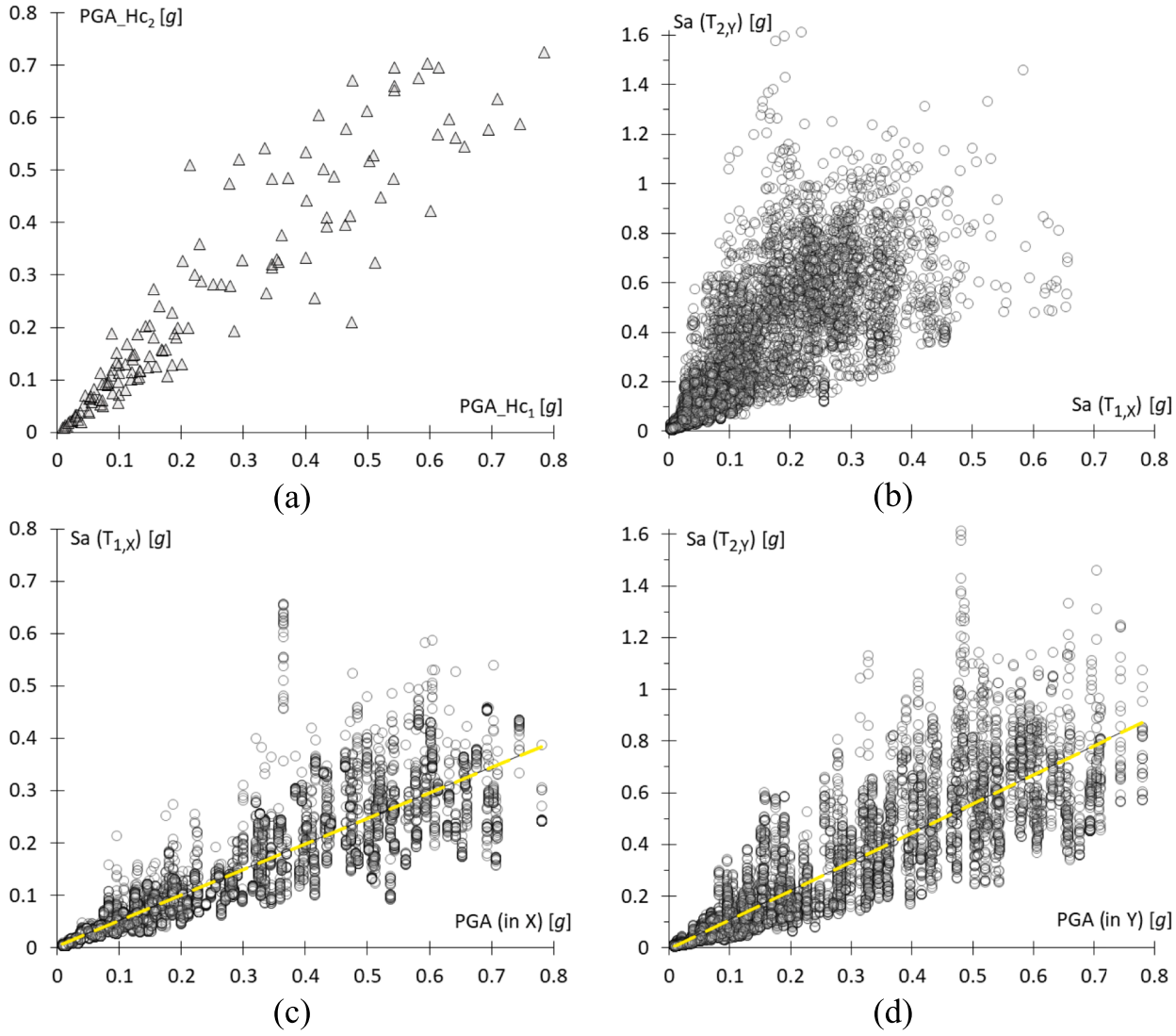

Fig. 9. Information on selected bidirectional records: (a) PGA values for the two horizontal components, Hc_1 and Hc_2; (b) S_a values for the main vibration periods, $T_{1,X}$ and $T_{2,Y}$; (c) $S_a(T_{1,X})$ versus PGA; (d) $S_a(T_{2,Y})$ versus PGA.

S_a, where N is the number of case study racks and the factor 2 is due to the two main vibration periods.

As can be seen from Fig. 9b, the values of $S_a(T_{1,X})$ are lower than those of PGA (about half); in contrast, the values of $S_a(T_{2,Y})$ are generally comparable to those of PGA, or even amplified in several cases. This is justified by the fact that $T_{1,X}$ and $T_{2,Y}$ are very different for these structures, with $T_{1,X}$ ranging from about 1.9 to 5.1 s and $T_{2,Y}$ from about 0.7 to 1.5 s. To better visualize the filtering effect of the seismic acceleration provided by the racks in the two directions, Fig. 9c and 9d show the values of $S_a(T_{1,X})$ and $S_a(T_{2,Y})$, respectively, versus PGA values.

4. Seismic fragility results

This section first presents the overall fragility of the analysed rack stock, examining the damage modes of these structures by comparing the various EDPs and IMs (subsection 4.1). Given the size of the stock, this average fragility should also cover to some extent the epistemic uncertainties of individual racks (related, for example, to material properties, profile and connection characteristics, element imperfections, etc.), which were not explicitly evaluated in this study.

Then, fragility curves are shown for subsets of racks (subsection 4.2), defined by varying one main structural parameter at a time (i.e., total height H, distance between load levels h, and type of upright U). From these results, some useful considerations can be drawn both on the effect of these parameters on fragility and on the homogeneity of the selected structures in relation to their seismic behaviour.

Lastly, fragility is also represented through additional EDPs, which quantify the dropping of certain volumes (in %) of pallets and the yielding of certain amounts (in %) of *btc* connections (subsection 4.3). Such a fragility representation could be useful for more refined estimates of expected seismic losses of companies.

4.1. Seismic fragility of the entire stock

Figs. 10 and 11 show, for the entire rack stock, the fragility sets (i.e., the fragility curves for all DSs) conditional on PGA and S_a, respectively, associated with the various EDPs: (a) ε^*, (b) φ_{btc}, (c) θ_X, and (d) φ_{base}. Table 8 and 9 show the parameters of the related lognormal functions, i.e., median (μ_{PGA}, μ_{Sa}) and logarithmic standard deviation (β_{PGA}, β_{Sa}) for both IMs.

In addition to the DS1, DS2, and DS3 curves, the "NonC" and "Collapse" curves are also shown in the case of ε^*, which show the probability of numerical non-convergence and the actual probability of structural collapse, respectively (as explained in subsection 3.2). The

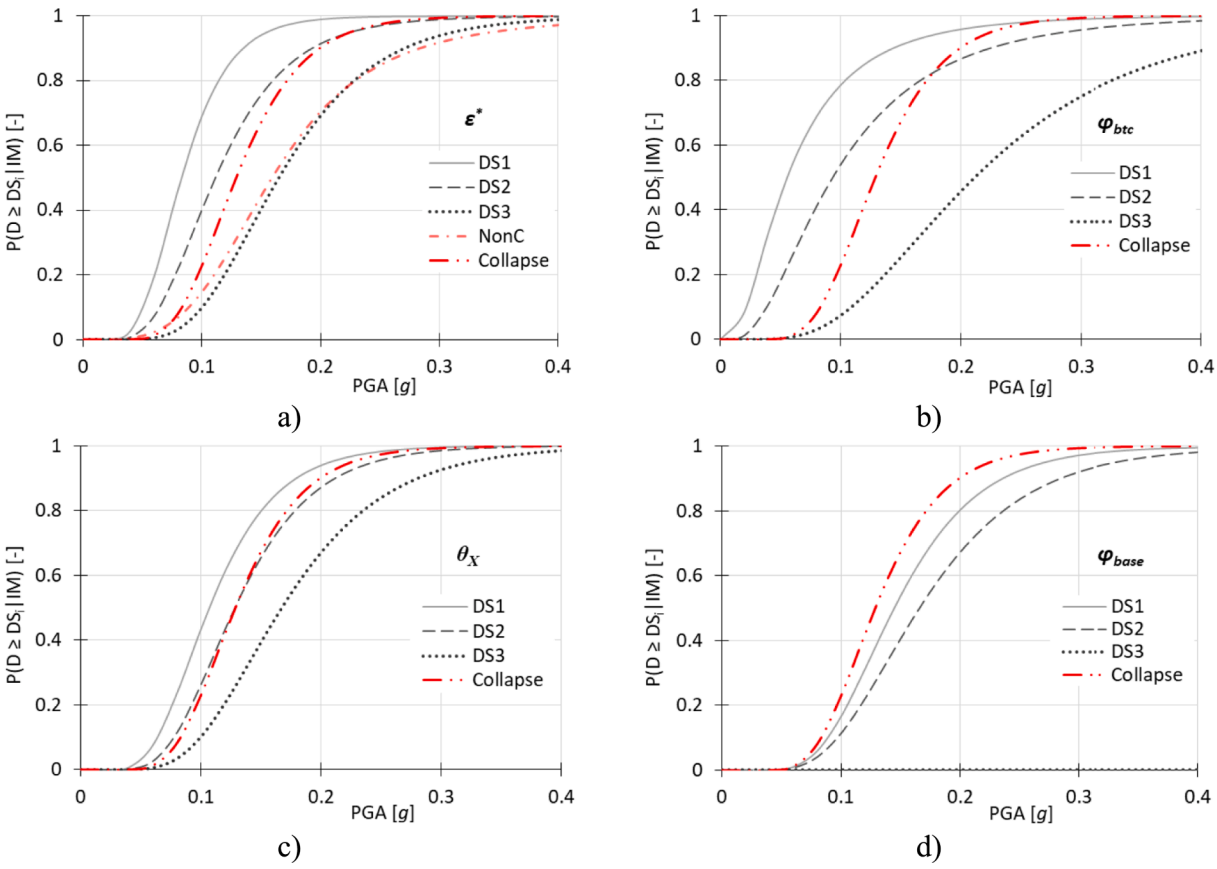

Fig. 10. Rack stock fragility conditional on PGA: (a) ε^*, (b) φ_{btc}, (c) θ_X, and (d) φ_{base}.

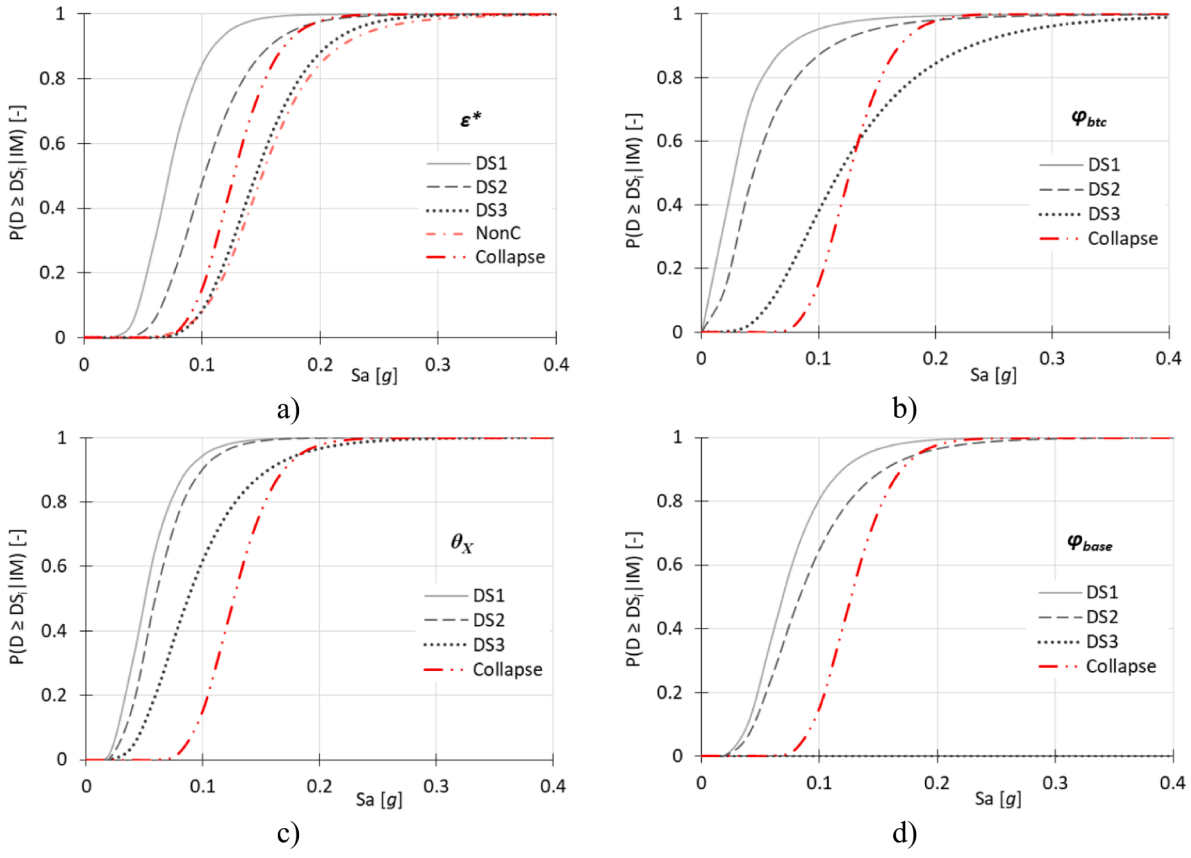

Fig. 11. Rack stock fragility conditional on S_a: (a) ε^*, (b) φ_{btc}, (c) θ_X, and (d) φ_{base}.

Table 8
Median (μ_{PGA}) and logarithmic standard deviation (β_{PGA}) in PGA, for all EDPs and DSs.

EDP:	DS1		DS2		DS3		Collapse	
	μ_{PGA} (g)	β_{PGA} (−)	μ_{PGA} (g)	β_{PGA} (−)	μ_{PGA} (g)	β_{PGA} (−)	μ_{PGA} (g)	β_{PGA} (−)
ε^*	0.083	0.378	0.112	0.427	0.165	0.385	0.129	0.340
φ_{btc}	0.055	0.748	0.093	0.689	0.211	0.517	–	–
θx	0.107	0.405	0.128	0.393	0.167	0.405	–	–
φ_{base}	0.144	0.380	0.165	0.420	–	–	–	–

Table 9
Median (μ_{Sa}) and logarithmic standard deviation (β_{Sa}) in S_a, for all EDPs and DSs.

EDP:	DS1		DS2		DS3		Collapse	
	μ_{Sa} (g)	β_{Sa} (−)	μ_{Sa} (g)	β_{Sa} (−)	μ_{Sa} (g)	β_{Sa} (−)	μ_{Sa} (g)	β_{Sa} (−)
ε^*	0.071	0.337	0.101	0.340	0.145	0.272	0.127	0.228
φ_{btc}	0.027	0.790	0.044	0.726	0.117	0.525	–	–
θx	0.050	0.406	0.059	0.406	0.087	0.457	–	–
φ_{base}	0.069	0.434	0.083	0.486	–	–	–	–

"Collapse" curve (calculated through the parameter ε^*) is then plotted in the fragility sets of the other EDPs for comparison purposes.

Looking at the fragility results in PGA (Fig. 10), the following considerations can be made.

- The fragility associated with ε^* demonstrates the high seismic vulnerability of these structural systems, showing relatively low median values (μ_{PGA}) compared to those of common building structures. In addition, the rather narrow fragility interval between the DS2 ($\mu_{PGA} = 0.112$ *g*) and Collapse ($\mu_{PGA} = 0.129$ *g*) curves clearly shows the poor redundancy and ductile capacity of these structures. It is also interesting to note the good overlap between the DS3 (collapse with convergent analyses) and NonC (non-convergent analyses) curves, which indicates that the cause of non-convergence is indeed an excessive strain in the upright sections.
- The Collapse curve ($\mu_{PGA} = 0.129$ *g*) always anticipates the DS3 curves of the other EDPs (φ_{btc}, θ_X, φ_{base}), and this proves that ε^* is the EDP that generally drives the collapse of these racks. This also means that for earthquakes with prevailing excitation in the *X* direction, these racks would appear less vulnerable. Moreover, among the EDPs representing rack deformation in the down-aisle direction, θ_X is the one that first reaches DS3 ($\mu_{PGA} = 0.167$ *g*), and thus the one that best interprets the overall rack damage due to high deflections in that direction.
- The Collapse curve then turns out to be very similar to the DS2 curve of θ_X ($\mu_{PGA} = 0.128$ *g*), indicating that the probabilities of reaching upright failure and yield drift ($\theta_{X,y}$) are similar. This outcome is also interesting to interpret and compare relevant results in the literature based on 2D rack models and analyses in the down-aisle direction only.
- Comparing the fragility associated with φ_{btc} and θ_X, it is observed that the μ_{PGA} values related to φ_{btc} are lower than those related to θ_X for DS1 ($0.055\ g < 0.107\ g$) and DS2 ($0.093\ g < 0.128\ g$), while the opposite is noted for DS3 ($0.211\ g > 0.167\ g$). This is motivated by the fact that once DS2 (yielding) of the *btc* connections is achieved, the inter-storey stiffness of the racks in the *X* direction is greatly reduced, causing a rapid increase in the θ_X values. In addition, the distance between DS2 and DS3 of φ_{btc} ($\mu_{PGA} = 0.093$–0.211 *g*) denotes some dissipative capacity of *btc* connections, which, however, cannot be fully exploited because Collapse is reached before DS3.
- The fragility associated with φ_{base} is the lowest among the selected EDPs. Specifically, DS1 of base connections ($\mu_{PGA} = 0.144$ *g*) is attained later than DS2 of θ_X ($\mu_{PGA} = 0.128$ *g*) and φ_{btc} ($\mu_{PGA} = 0.093$ *g*). Lastly, DS3 is never reached for φ_{base} because of the numerical non-convergence (due to large strains in the upright sections). All this seems reasonable and indicates a certain and appropriate hierarchy of resistances among the structural elements of these storage systems.

On the other hand, from the fragility results in S_a (Fig. 11), the following observations can be drawn.

- The acceleration range within which the fragility curves of ε^* develop is similar in PGA and S_a. This result is interesting, also considering that ε^* is the most effective EDP for assessing the safety of these racks, and allows direct comparison of literature results obtained from different approaches, in PGA or S_a.
- On the contrary, the acceleration range relative to the development of fragility curves for the other EDPs (φ_{btc}, θ_X, φ_{base}) is approximately halved when switching from PGA to S_a. This is clearly due to the high vibration periods of these racks in the down-aisle direction ($T_{1,X}$), which provide a beneficial filtering effect on seismic acceleration. In fact, the same accelerograms yield much lower S_a values in the *X* direction than in the *Y* direction, resulting in median values associated with φ_{btc}, θ_X, and φ_{base} that are also lower (about half) when expressed in S_a instead of PGA. In other words, the lower resistance of these structures in the down-aisle direction is counterbalanced by the beneficial effect of the high vibration periods in the same direction.
- Based on the above, the Collapse curve is no longer directly comparable with the fragility sets of EDPs in the down-aisle direction. This comparison, still of interest, requires considering that the Collapse curve is derived from the values of S_a recorded in the cross-aisle direction.
- Lastly, regarding the comparison of the fragility sets of φ_{btc}, θ_X, and φ_{base}, the same observations made for the fragility conditional on PGA generally apply.

4.2. Seismic fragility of rack subsets

Figs. 12 to 15 show and compare, for the various EDPs, the conditional fragility on S_a of various rack subsets, defined by selecting all case study racks with the same (a) upright section (U_1, U_2, U_3), (b) load-level height (h_1, h_2, h_3), and (c) total height (H_1, H_2, H_3). Specifically, fragility curves are shown for DS1, DS2, and Collapse in the case of ε^* (Fig. 12), and only for DS2 in the other cases of φ_{btc} (Fig. 13), θ_X (Fig. 14), and φ_{base} (Fig. 15), for a better visualization. The following are the main observations that emerge from these figures.

- To understand the effect of the upright cross-section (*U*) on fragility, it should be recalled that both the strength and stiffness of the uprights increase slightly from *U1* to *U2* and increase strongly from *U2*

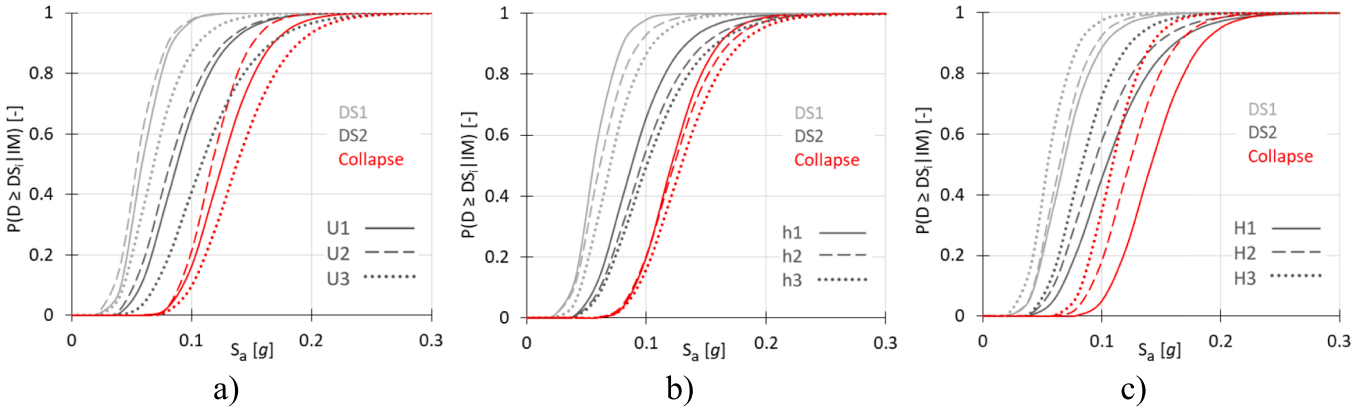

Fig. 12. Fragility curves of rack subsets with the same (a) U, (b) h, and (c) H, for the EDP ε^*.

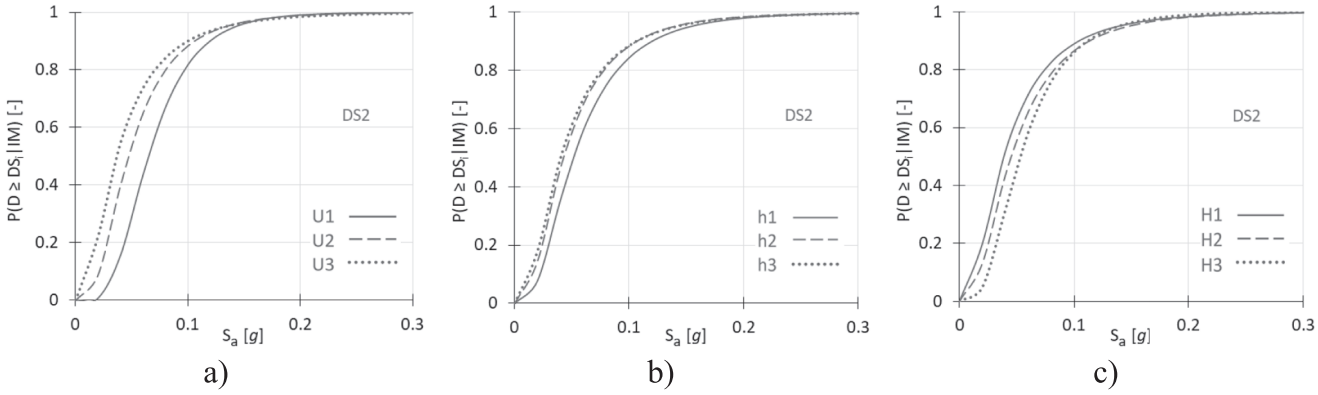

Fig. 13. Fragility curves of rack subsets with the same (a) U, (b) h, and (c) H, for the EDP φ_{btc}.

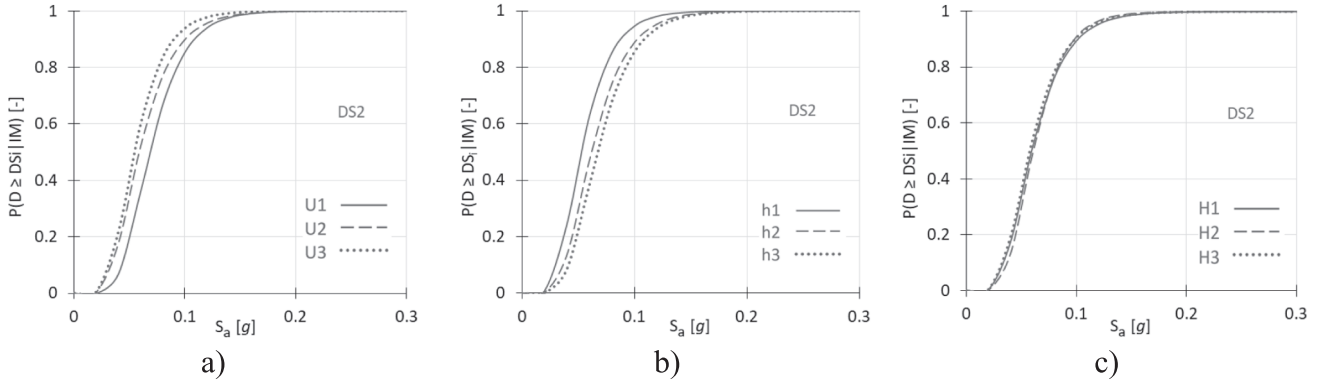

Fig. 14. Fragility curves of rack subsets with the same (a) U, (b) h, and (c) H, for the EDP θ_X.

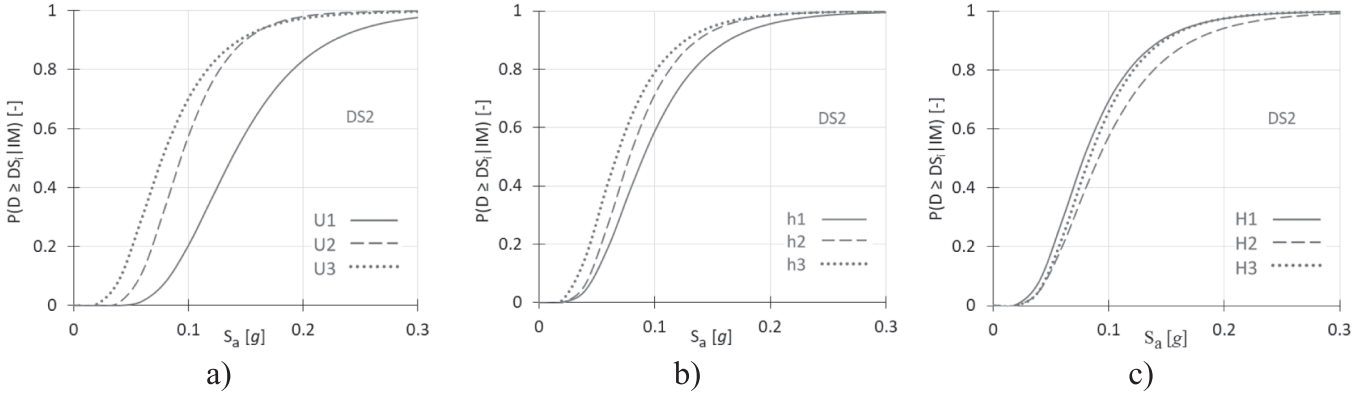

Fig. 15. Fragility curves of rack subsets with the same (a) U, (b) h, and (c) H, for the EDP φ_{base}.

to *U3*, with the latter profile being installed with the highest performing *btc* connection (*btc2*). The increase in stiffness (*U1* to *U3*) attracts higher spectral accelerations (S_a) due to the reduction in vibration periods. Furthermore, the increase in strength (*U1* to *U3*) results in higher pallet loads, which were assumed to be proportional to the load-bearing capacity of the transverse frames. Higher pallet loads do not necessarily lead to an increase in seismic forces (especially in the cross-aisle direction), as they also significantly increase the vibration periods. All this affects the rack fragility in a way that is difficult to anticipate. For ε^* (Fig. 12a), the median value at Collapse (μ_{Sa_C}) for *U2* (0.117 *g*) is lower than that for *U1* (0.126 *g*), indicating the dominance of the negative effects of section increase; whereas, in the case of *U3*, the μ_{Sa_C} value is the highest (0.138 *g*), i.e., positive effects prevail. In contrast, for the other EDPs in the *X* direction (Fig. 13a, 14a, 15a), fragility always increases from *U1* to *U3*, i.e., negative effects always prevail; specifically, the median values at DS2 (μ_{Sa_DS2}) ranges from 0.065 to 0.036 *g* for φ_{btc}, from 0.068 to 0.054 *g* for θ_X, and from 0.138 to 0.078 *g* for φ_{base}.

- As *h* increases, the load-bearing capacity of the transverse frames, and consequently the total load per upright, decrease almost linearly (see subsection 2.1). However, this load is distributed over a smaller number of load levels, resulting in an increased load per single load level. In addition, the vibration periods in the down-aisle direction slightly increase as *h* increases. For ε^* (Fig. 12b) and θ_X (Fig. 14b), this results in a reduction in fragility from *h1* to *h3* (with μ_{Sa_C} from 0.121 to 0.129 *g* for ε^*, and μ_{Sa_DS2} from 0.053 to 0.067 *g* for θ_X). This is reasonable considering the overall reduction in inertial forces due to the lower total load and longer vibration periods; moreover, as *h* increases, the yield drift limit ($\theta_{X,y}$) increases. In contrast, for rotational EDPs (Fig. 13b and 15b), fragility increases as *h* increases (with μ_{Sa_DS2} from 0.051 to 0.040 *g* for φ_{btc}, and from 0.091 to 0.067 *g* for φ_{base}). This is due to the higher load per load level and the longer effective length of the uprights in the *X* direction, leading to greater rotations.
- The increase in *H* raises the rack's overall centre of mass and increases the vibration periods in both directions of analysis. Then, the flexural deformability of the rack increases over the shear deformability as *H* increases. In addition, for the same *U* and *h*, and therefore the total load on the upright, the load per level is reduced from *H1* to *H3* because the number of levels increases. Overall, increasing the rack height leads to an increase in fragility associated with ε^* (Fig. 12c), because of the increased bending at the base of the uprights (μ_{Sa_C} from 0.141 to 0.109 *g*). In contrast, the other EDPs are affected differently by *H*. Specifically, the yielding of the *btc* connections (Fig. 13c) is postponed by the increase in *H* due to a lower load per level and lower S_a values (μ_{Sa_DS2} from 0.039 to 0.053 *g*). On the other hand, the yielding of the base connections (Fig. 15c) is postponed for racks with intermediate *H*, which results in a good compromise between the increase of flexural deformation and the reduction of S_a values. Lastly, the fragility associated with θ_X (Fig. 14c) does not appear to depend significantly on *H*, a rather interesting result.
- Lastly, the fragility variations involved are rather small, also in view of the limited extension of the S_a range in which the curves are defined. This confirms that the selected racks are homogeneous in terms of seismic vulnerability. Therefore, the average fragility of the

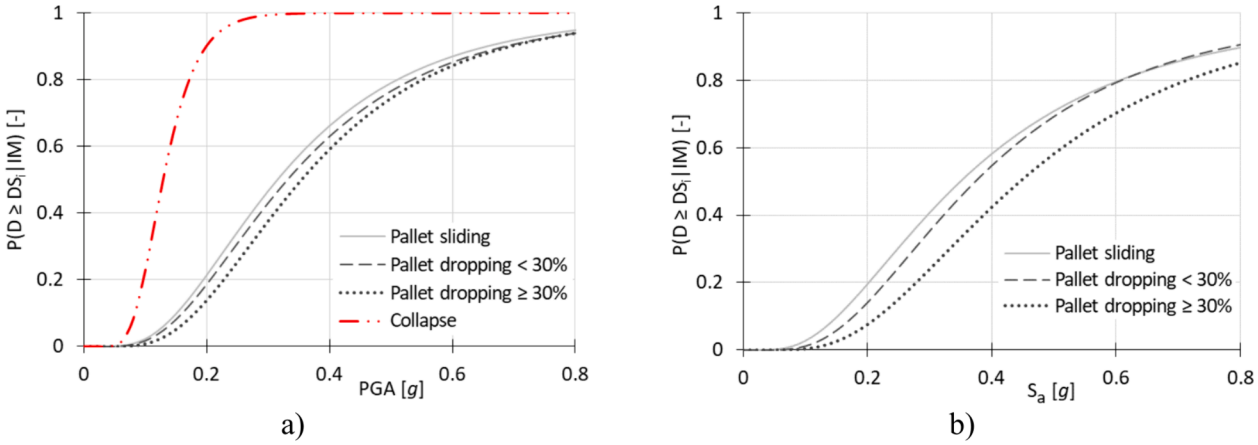

Fig. 16. Fragility curves of pallet sliding and pallet dropping (<30 %, ≥30 %): (a) PGA, (b) S_a.

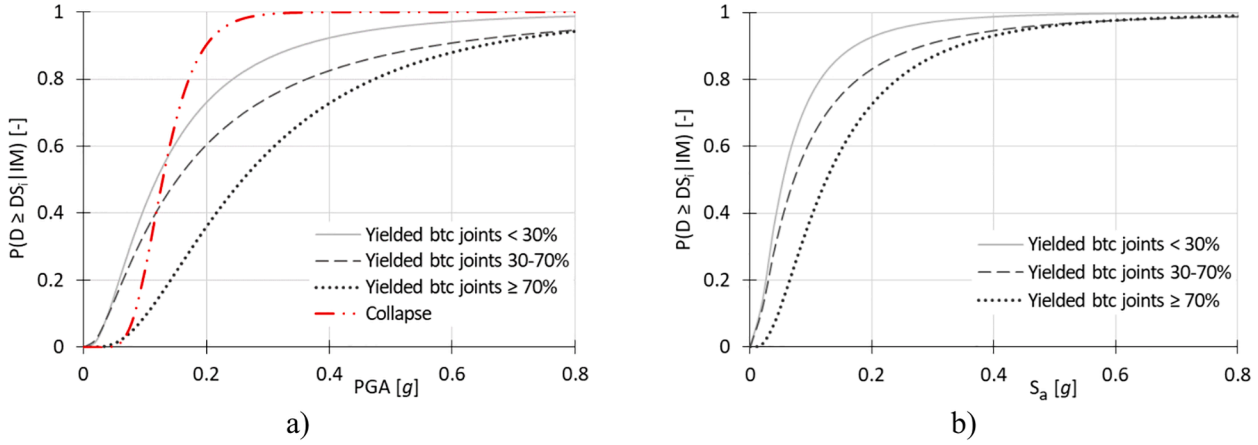

Fig. 17. Fragility curves of *btc* connection yielding (<30 %, 30–70 %, ≥70 %): (a) PGA, (b) S_a.

entire rack stock (Figs. 10 and 11) can be effectively used to assess the seismic vulnerability of these structures, even considering the significant uncertainties in the definition of the seismic input and the non-linear modelling. In addition, the dispersion introduced by the variation of the structural parameters (i.e., *U*, *h*, *H*), also considering their different effect on the various EDPs, makes the stock fragility results particularly robust for spatial-scale risk estimates.

4.3. Insight into damage to pallet and btc connections

Figs. 16 and 17 show the rack stock fragility associated with additional EDPs, which quantify the damage to pallet (Fig. 16) and *btc* connections (Fig. 17). This fragility was calculated on the results of all TH analyses (both convergent and non-convergent). Specifically, Fig. 16 shows the fragility curves that provide the probability of triggering pallet sliding and dropping certain amounts of pallets, i.e., (*i*) from one pallet to 30 % of the total pallets and (*ii*) over 30 %. On the other hand, Fig. 17 shows the fragility curves associated with the yielding of certain amounts of *btc* connections, i.e., (*i*) from 1 joint to 30 % of the total joints, (*ii*) from 30 % to 70 %, and (*iii*) over 70 %. In both these figures, fragility is shown conditional on PGA (graphs a) and S_a (graphs b). Clearly, the fragility of the pallet is calculated with respect to IMs in the *Y* direction, whereas the fragility of the *btc* connections with respect to IMs in the *X* direction. Also, in the graphs with PGA, the Collapse curve is shown for comparison purposes. In general, these fragility results suggest the following observations.

- The sliding triggering curve correctly anticipates the pallet loss curves; however, they are very close, indicating that the pallet is very likely to fall because of sliding. Then, the median fragility values are slightly higher when expressed in S_a (0.349 to 0.445 *g*) instead of PGA (0.315 to 0.354 *g*). In addition, the curves in S_a are further apart compared to those in PGA, as S_a better represents the actual acceleration experienced by the pallets than PGA. In any case, for the case study racks, pallet fragility is significantly lower than structural fragility; indeed, the Collapse curve greatly anticipates the pallet loss curves.
- The fragility set in Fig. 17 is shifted to the left when conditional on S_a, due to the high vibration periods in the *X* direction (as already noted). In addition, the median values of the first damage curve "<30 %" (i.e., $\mu_{PGA} = 0.118\ g$ and $\mu_{Sa} = 0.054\ g$) are only slightly greater than those associated with the DS2 of φ_{btc} (i.e., $\mu_{PGA} = 0.093\ g$ and $\mu_{Sa} = 0.044\ g$, see Tables 8 and 9). This indicates that the damage to connections propagates quickly after the first connection yields. Lastly, the μ_{PGA} value of the Collapse curve (0.129 *g*) is intermediate between those of the "<30 %" and "30–70 %" curves (0.118–0.152 *g*), suggesting that racks collapse after yielding a significant amount of connections, which thus provide some energy dissipation, albeit limited.

5. Conclusions

The seismic fragility of a stock of 27 unbraced steel pallet racks was investigated in this paper. These racks are characterised by various upright sections (*U*), load level heights (*h*), and total heights (*H*), and are designed for gravity loads only, exhibiting similar levels of compression at the base of the uprights. Seismic fragility was derived through a cloud approach, based on TH analysis and non-linear 3D rack modelling. *Btc* and base connections were modelled via lumped plasticity, whereas the upright behaviour was simulated via distributed plasticity, also accounting for buckling. The full load condition was assumed in this study and a friction model was implemented under each pallet mass to simulate its possible sliding. 268 bidirectional seismic inputs, representative of Italian seismicity on rigid soil, were selected, thus performing a total of 7236 TH analyses in the OpenSees environment.

For both the entire rack stock and subsets of it (defined by varying *U*, *h*, and *H*), multiple sets of fragility were derived, associated with various engineering demand parameters (EDPs) and conditional on two seismic intensity measures (IMs), i.e., PGA and S_a. These EDPs were an overall (axial-flexural) strain parameter of the uprights (ε^*), the drift between load levels in the down-aisle direction (θ_X), and the rotations of the *btc* (φ_{btc}) and base (φ_{base}) connections around the *Y* axis. For each EDP, fragility was defined for three damage states, representing incipient damage (DS1), yielding state (DS2) and incipient collapse (DS3). To correctly assess the rack failure, information from non-convergent analyses (due to excessive strains in the upright sections) was also taken into account and a specific Collapse curve was derived. Lastly, fragility was also represented through additional EDPs, associated with the dropping of certain pallet volumes and the yielding of certain amounts of *btc* connections.

Overall, the main conclusions of the study are as follows.

- ε^* is the EDP that best represented the seismic fragility of these racks, driving their structural collapse. In particular, the median values at Collapse, in PGA ($\mu_{PGA} = 0.129\ g$) and S_a ($\mu_{Sa} = 0.127\ g$), were significantly low, demonstrating the high seismic vulnerability of these systems. Furthermore, the rather narrow DS2-Collapse fragility range also demonstrated the low redundancy and ductile capacity of these structures.
- Among the EDPs representing rack deformation in the down-aisle direction (φ_{btc}, θ_X, φ_{base}), θ_X best interpreted the overall rack damage due to high deflections in that direction. In addition, the DS2 curve of θ_X was found to be very similar to the Collapse curve (ε^*), indicating that the probabilities of reaching the yield drift ($\theta_{X,y}$) and the upright failure (due to compression and biaxial bending) are equivalent.
- The fragility associated with φ_{btc} was greater than that associated with θ_X at DS1 and DS2; vice versa at DS3. This means that the *btc* connections were damaged first; then, once their yield strength was reached, the values of θ_X increased rapidly due to the reduction of inter-storey stiffness in the *X* direction, reaching the collapse drift prior to the failure of the *btc* connections. In addition, the fragility associated with φ_{base} is the lowest among the selected EDPs. All this reveals a certain hierarchy of resistances among the main structural elements of the rack.
- Although S_a better represents the seismic acceleration experienced by racks than PGA, the latter is independent of the structure and is generally employed to perform spatial-scale risk analyses, being more practical. The use of the cloud approach made it easy to derive the conditional fragility on both IMs. Whereas the fragility in PGA revealed the damage and collapse modes of the racks, the fragility in S_a showed more directly the resistance of the rack elements. In particular, the fragility associated with ε^* did not vary appreciably using PGA or S_a; in contrast, the fragility associated to the EDPs in the *X* direction increased greatly when expressed in S_a (the acceleration range of the fragility curves being approximately halved). This is clearly due to the high vibration periods of these racks in the down-aisle direction ($T_{1,X}$).
- The fragility results for rack subsets, which include all structures with the same upright, or load level height, or total height, made it possible to evaluate the effects of these structural parameters on fragility. These effects are not easily generalisable and are not homogenous across EDPs. However, the observed fragility variations are rather modest, confirming the homogeneity of the investigated racks in terms of seismic vulnerability and thus the effectiveness of the derived fragility models for the entire rack stock.
- The study on pallet fragility showed that pallet loss has a much lower probability of occurrence than structural collapse, so it is not a major problem for these racks. Lastly, the study on the damage propagation to *btc* connections showed that the rack collapse occurs with a large amount of yielded *btc* connections (>30 %), which therefore allow for some energy dissipation, albeit limited.

Future work will focus on analysing the fragility of other rack stocks (e.g., racks equipped with vertical bracing systems) and evaluating the effects of soft or amplifying soils, as well as innovative retrofit techniques [e.g., [56,57]], on their fragility. The ultimate goal is to develop adequate and efficient fragility models to support the assessment and management of industrial seismic risk, from the scale of individual companies to industrial areas.

CRediT authorship contribution statement

Marco Donà: Conceptualization, Data curation, Methodology, Software, Validation, Visualization, Writing – original draft, Writing – review & editing. **Giacomo Piredda:** Formal analysis, Software, Writing – original draft. **Alberto Zonta:** Data curation, Formal analysis, Methodology, Visualization. **Enrico Bernardi:** Data curation, Software. **Francesca da Porto:** Funding acquisition, Supervision.

Declaration of competing interest

The authors declare that they have no known competing financial interests or personal relationships that could have appeared to influence the work reported in this paper.

Data availability

Data will be made available on request.

Acknowledgements

This work was supported by the program "POR FSE VENETO 2014-2020", through the project 2105-0031-14632019, with the title: "Innovative technologies for the mitigation of the effects of dynamic actions on storage/racks systems". This study was also carried out within the RETURN Extended Partnership and received funding from the European Union Next-GenerationEU (National Recovery and Resilience Plan – NRRP, Mission 4, Component 2, Investment 1.3 – D.D. 1243 2/8/2022, PE0000005).Finally, this work was partially funded by ReLUIS and the Italian Department of Civil Protection, in the framework of the ReLUIS-DPC Project 2024-2026 (Work Package 4, Task 7: Industrial Buildings). Special thanks to Marco Ceresara (PhD Student) for supporting the validation of the parametric framework.

References

[1] CEN (European Committee for Standardization). 2005a. "EN 1993-1-8. Eurocode 3: Design of steel structures – Part 1-8: Design of joints." Brussels: CEN.
[2] CEN (European Committee for Standardization). EN 15512. Steel Static Storage Systems – Adjustable Pallet Racking Systems – Principles for structural design. Brussels: CEN; 2020.
[3] CEN (European Committee for Standardization). EN 16681. Steel Static Storage Systems – Adjustable Pallet Racking Systems – Principles for seismic design. Brussels: CEN; 2016.
[4] CEN (European Committee for Standardization). 2005b. "EN 1993-1-1. Eurocode 3: Design of steel structures – Part 1-1: General rules and rules for buildings." Brussels: CEN.
[5] Padilla-Llano DA, Moen CD, Eatherton MR. Cyclic axial response and energy dissipation of cold-formed steel framing members. Thin-Walled Struct 2014;78:95–107.
[6] Padilla-Llano DA, Eatherton MR, Moen CD. Cyclic flexural response and energy dissipation of cold-formed steel framing members. Thin-Walled Struct 2016;98:518–32.
[7] Affolter C, Piskoty G, Wullschleger L, Weisse B. Collapse of a high storage rack. Eng Fail Anal 2009;16(6):1846–55.
[8] Dubina D, Marginean I, Dinu F. Impact modelling for progressive collapse assessment of selective rack systems. Thin-Walled Struct 2019;143:106201.
[9] Perrone D, Calvi PM, Nascimbene R, Fischer EC, Magliulo G. Seismic performance of non-structural elements during the 2016 Central Italy earthquake. Bull Earthq Eng 2019;17(10):5655–77.
[10] Brown C, Stevenson J, Giovinazzi S, Seville E, Vargo J. Factors influencing impacts on and recovery trends of organizations: evidence from the 2010/2011 Canterbury earthquakes. Int J Disaster Risk Reduct 2015;14:56–72.
[11] Donà M, Bizzaro L, Carturan F, da Porto F. Effects of business recovery strategies on seismic risk and cost-effectiveness of structural retrofitting for business enterprises. Earthq Spectra 2019;35(4):1795–819.
[12] Braga F, Gigliotti R, Monti G, Morelli F, Nuti C, Salvatore W, et al. Speedup of post earthquake community recovery: the case of precast industrial buildings after the Emilia 2012 earthquake. Bull Earthq Eng 2014;12(5):2405–18.
[13] Bernuzzi C, Castiglioni CA. Experimental analysis on the cyclic behaviour of beam-to-column joints in steel storage pallet racks. Thin-Walled Struct 2001;39(10):841–59.
[14] Yin L, Tang G, Zhang M, Wang B, Feng B. Monotonic and cyclic response of speed-lock connections with bolts in storage racks. Eng Struct 2016;116:40–55.
[15] Dai L, Zhao X, Rasmussen KJ. Flexural behaviour of steel storage rack beam-to-upright bolted connections. Thin-Walled Struct 2017;124:202–17.
[16] Dai L, Zhao X, Rasmussen KJ. Cyclic performance of steel storage rack beam-to-upright bolted connections. J Constr Steel Res 2018;148:28–48.
[17] Zhao X, Dai L, Rasmussen KJ. Hysteretic behaviour of steel storage rack beam-to-upright boltless connections. J Constr Steel Res 2018;144:81–105.
[18] Gusella F, Lavacchini G, Orlando M. Monotonic and cyclic tests on beam-column joints of industrial pallet racks. J Constr Steel Res 2018;140:92–107.
[19] Jovanović Đ, Žarković D, Vukobratović V, Brujić Z. Hysteresis model for beam-to-column connections of steel storage racks. Thin-Walled Struct 2019;142:189–204.
[20] Yin L, Tang G, Li Z, Zhang M. Responses of cold-formed steel storage racks with spine bracings using speed-lock connections with bolts II: Nonlinear dynamic response history analysis. Thin-Walled Struct 2018;125:89–99.
[21] Yin L, Tang G, Li Z, Zhang M, Feng B. Responses of cold-formed steel storage racks with spine bracings using speed-lock connections with bolts I: Static elastic-plastic pushover analysis. Thin-Walled Struct 2018;125:51–62.
[22] Gabbianelli G, Francesco C, Nascimbene R. Seismic vulnerability assessment of steel storage pallet racks. Ingegneria Sismica 2020;37(2).
[23] Baldassino, N., & Zandonini, R. 2008. "Performance of base-plate connections of steel storage pallet racks." In *Proceedings of Fifth International Conference on Coupled Instabilities in Metal Structures (CIMS2008), Gregory J. Hancock Symposium, Sydney, Australia* (pp. 119-130).
[24] Petrone F, Higgins PS, Bissonnette NP, Kanvinde AM. The cross-aisle seismic performance of storage rack base connections. J Constr Steel Res 2016;122:520–31.
[25] Huang Z, Wang Y, Zhao X, Sivakumaran KS. Determination of the flexural behavior of steel storage rack baseplate upright connections with eccentric anchor bolts. Thin-Walled Struct 2021;160:107375.
[26] Jacobsen E, Tremblay R. Shake-table testing and numerical modelling of inelastic seismic response of semi-rigid cold-formed rack moment frames. Thin-Walled Struct 2017;119:190–210.
[27] FEMA (Federal Emergency Management Agency). 2005. "FEMA 460. Seismic Considerations for Steel Storage Racks Located in Areas Accessible to the Public". National Institute of Building Sciences, Washington D.C., 2005.
[28] Krawinkler, H., Cofie, N. G., Astiz, M. A., & Kircher, C. A. 1979. "Experimental Study on the Seismic Behavior of Industrial Storage Racks". Report No. 41, The John A. Blume Earthquake Engineering Center, Department of Civil Engineering, Stanford University, Stanford, CA, 139 p.
[29] Chen C. K., Scholl R. E., & Blume J. A. 1980. "Seismic Study of Industrial Steel Storage Racks". Report prepared for the National Science Foundation and for the Rack Manufacturers Institute and Automated Storage and Retrieval Systems by URS/John A. Blume & Associates, San Francisco, CA, 569 p.
[30] Filiatrault, A. 2001. "Shake-Table Tests of Storage Racks and Contents". Presentation material at the April 12, 2001 Seismic Safety Commission Hearing on Industrial Storage Racks, San Francisco, CA.
[31] Filiatrault, A. & Wanitkorkul, A. 2004. "Shake-Table Testing of Frazier Industrial Storage Racks". Report No. CSEE-SEESL-2005-02, Structural Engineering and Earthquake Simulation Laboratory, Departmental of Civil, Structural and Environmental Engineering, University at Buffalo, State University of New York, 83 p.
[32] Higgins P. Personal Communication. Malibu, CA: Peter Higgins and Associates; 2004.
[33] Proença, J., Rosin, I., Calado, L. 2009. "Storage racks in seismic areas". European Commission, Directorate-General for Research and Innovation. Publications Office. https://data.europa.eu/doi/10.2777/60886.
[34] Drei, A., Rovere, L., Vayas, I., et al. 2016. "Seismic behaviour of steel storage pallet racking systems (SEISRACKS2): final report". European Commission, Directorate-General for Research and Innovation. Publications Office. https://data.europa.eu/doi/10.2777/686466.
[35] European Racking Federation, 2011. FEM Document 10.2.08. "Recommendations for the design of static steel pallet racks in seismic conditions" – Version 1.04 – May 2011. https://www.fem-rands.org/publications.

[36] Castiglioni CA, Drei A, Kanyilmaz A, Mouzakis HP. Earthquake-induced pallet sliding in industrial racking systems. J Build Eng 2018;19:122–33.
[37] Sideris P, Filiatrault A, Leclerc M, Tremblay R. Experimental Investigation on the Seismic Behavior of Palletized Merchandise in Steel Storage Racks. Earthq Spectra 2010;26(1):209–33.
[38] Nuñez E, Aguayo C, Mata R. Incremental dynamic analysis of steel storage racks subjected to Chilean earthquakes. Thin-Walled Struct 2023;182:110288. https://doi.org/10.1016/j.tws.2022.110288.
[39] Bernuzzi C, Petrushevska S, Simoncelli M. QUSDRA approach: quick seismic design of steel storage racks. Ingegneria Sismica (Int J Earthquake Eng) 2022;39(1):1–22.
[40] Tsarpalis D, Vamvatsikos D, Delladonna F, Fabini M, Hermanek J, Margotan PD, et al. Macro-characteristics and taxonomy of steel racking systems for seismic vulnerability assessment. Bull Earthq Eng 2022;20(5):2695–718.
[41] Zonta, A. 2023. "Seismic vulnerability of industrial steel pallet racks: development of fragility curves for existing and retrofitted configurations." Ph.D. Thesis, University of Padova, XXXV cycle.
[42] McKenna F, Fenves GL, Scott MH. Open system for earthquake engineering simulation. Berkeley, CA: University of California; 2000.
[43] Neuenhofer A, Filippou FC. Evaluation of nonlinear frame finite-element models. J Struct Eng 1997;123(7):958–66.
[44] Scott MH, Fenves GL. Plastic hinge integration methods for force-based beam–column elements. J Struct Eng 2006;132(2):244–52.
[45] FEMA (Federal Emergency Management Agency) 461. 2007. "Interim testing protocols for determining the seismic performance characteristics of structural and nonstructural components." Washington, DC: FEMA.
[46] Menegotto, M., & Pinto, P.E. 1973. "Method of analysis of cyclically loaded RC plane frames including changes in geometry and non-elastic behavior of elements under normal force and bending." *Proceedings of IABSE Symposium*, Lisbon, Portugal.
[47] Bernuzzi C, Gobetti A, Gabbianelli G, Simoncelli M. Warping influence on the resistance of uprights in steel storage pallet racks. J Constr Steel Res 2014;101:224–41. https://doi.org/10.1016/j.jcsr.2014.05.014.
[48] Bernuzzi C, Pieri A, Squadrito V. Warping influence on the static design of unbraced steel storage pallet racks. Thin-Walled Struct 2014;79:71–82. https://doi.org/10.1016/j.tws.2014.01.024.
[49] Baker JW. Probabilistic structural response assessment using vector-valued intensity measures. Earthq Eng Struct Dyn 2007;36(13):1861–83.
[50] Saler E., Carpanese P., Follador V., da Porto F. 2021. "Derivation of seismic fragility curves of a gravity-load designed RC school building through NLTHA." 8th International Conference on Computational Methods in Structural Dynamics and Earthquake Engineering (CompDyn 2021), Streamed from Athens, Greece.
[51] Jalayer F, Ebrahimian H, Miano A, Manfredi G, Sezen H. Analytical Fragility Assessment Using Unscaled Ground Motion Records. Earthq Eng Struct Dyn 2017;46(15):2639–63.
[52] Manfredi V, Masi A, Özcebe AG, Paolucci R, Smerzini C. Selection and spectral matching of recorded ground motions for seismic fragility analyses. Bull Earthq Eng 2022:1–27.
[53] Paolucci R., Ozcebe A.G., Smerzini C., Masi A., Manfredi V. 2020. "Selection and spectral matching of recorded ground motions for earthquake engineering analysis." Available at: http://143.225.144.186:5000/.
[54] Smerzini C, Galasso C, Iervolino I, Paolucci R. Ground motion record selection based on broadband spectral compatibility. Earthq Spectra 2014;30(4):1427–48.
[55] MIT (Italian Ministry of Infrastructure and Transport). 2018. Update of the "Technical Standards for Constructions". DM 2018/01/17, "S.O. No. 8 alla G.U. del 20 Febbraio 2018, No. 32", Rome, Italy (in Italian).
[56] Donà M, Bernardi E, Zonta A, Ceresara M, da Porto F. Effectiveness of load-level isolation system for pallet racking systems. Front Built Environ 2022;8:944026. https://doi.org/10.3389/fbuil.2022.944026.
[57] Bernardi E, Donà M, Tan P, da Porto F. Optimal design method of the load-level isolation system for industrial steel racking. J Constr Steel Res 2023;210:108096. https://doi.org/10.1016/j.jcsr.2023.108096.